ARMY RESEARCH LABORATORY

A One-Dimensional Numerical Method for Simulating Multiple Stage Shock Tube Flows

Stephen J. Schraml

ARL-TR-1255 NOVEMBER 1996

The findings in this report are not to be construed as an official Department of the Army position unless so designated by other authorized documents.

Citation of manufacturer's or trade names does not constitute an official endorsement or approval of the use thereof.

Destroy this report when it is no longer needed. Do not return it to the originator.

Abstract

A method is presented for the numerical simulation of time-dependent fluid flow in shock tubes and blast simulators. This method solves the Euler equations in a one-dimensional (1-D) computational domain with area changes. Complex flow fields can be simulated through the use of grid geometries and boundary conditions that are allowed to vary with time. The formulation of the solution algorithm and the time-varying boundary conditions are described. Results of a set of benchmark calculations are presented to illustrate the capabilities of the technique.

Army Research Laboratory
Aberdeen Proving Ground, MD 21005-5425

ARL-TR-1255 November 1996

A One-Dimensional Numerical Method for Simulating Multiple Stage Shock Tube Flows

Stephen J. Schraml
Weapons & Materials Research Directorate

ACKNOWLEDGMENTS

This report documents the validation of a numerical method for simulating blast flows. This validation was made possible by the availability of experimental data from several unique shock tube facilities. The test data from the U.S. Army Research Laboratory (ARL) 57-cm shock tube were provided to the author by Mr. Peter Muller of ARL. The experiments in the ARL 2.44-m blast simulator were performed under the direction of Mr. John Sullivan of ARL. The initial conditions and test results from this facility were collected and made available by Ms. Audrey Mihalcin of ARL. The test data from the LB/TS was provided by Mr. Edward Martinez of the Defense Special Weapons Agency (DSWA).

Most of the calculations presented in this report were performed by Mr. Ashutosh Jhaveri whose efforts made possible the timely publication of this report. Mr. Bernard Guidos of ARL performed a technical review of the manuscript and provided many valuable comments to enhance its overall clarity and technical integrity. The author gratefully acknowledges the efforts and support of these individuals.

INTENTIONALLY LEFT BLANK

TABLE OF CONTENTS

INTENTIONALLY LEFT BLANK

LIST OF FIGURES

LIST OF FIGURES (continued)

LIST OF TABLES

INTENTIONALLY LEFT BLANK

1. TRANSIENT FLOW SIMULATION

The U.S. Army Research Laboratory (ARL) uses a variety of computational fluid dynamics (CFD) techniques for the numerical simulation of air blast.[1] High resolution simulations of blast flows are accomplished through the use of two-dimensional (2-D) and three-dimensional (3-D) Euler[2] and Navier-Stokes[3] flow solvers. Typical 2-D flow simulations require tens of hours of computer time to complete, while 3-D calculations can require hundreds of hours.[4] With high resolution, multi-dimensional simulation come huge data storage requirements and time-consuming data analysis. Some blast studies require the capability to estimate trends in flow field characteristics through parametric analysis. Often, this type of analysis consists of a large number of calculations that must be completed in a short period of time to address critical project issues.[5] To address this need, a flow solver has been developed to simulate transient, compressible fluid flow in a one-dimensional (1-D) computational domain with variable area. This new CFD tool is called the **T**ransient **O**ne-Dimensional **F**low **S**olver (TOFS). A description of the TOFS algorithm, code features, and the presentation of some validation test cases form the basis of this report.

2. GOVERNING EQUATIONS

The motion of a fluid can be completely described by the conservation of mass, momentum and energy. Conservation of momentum for an inviscid, Newtonian fluid is described by the Euler equation.[6] When gravitational effects are ignored, the Euler equation takes the general form

$$\rho \frac{Du_i}{Dt} = -\frac{\partial p}{\partial x_i} \tag{1}$$

in which x_i represents the spatial dimensions, and u_i represents the velocity components in these dimensions.

When applied in only one dimension, the conservation laws take the form of the partial differential equation[7] (PDE)

$$\frac{\partial \mathbf{q}}{\partial t} + \frac{\partial \mathbf{F}}{\partial x} = 0 \tag{2}$$

in which

$$\mathbf{q} = \begin{bmatrix} \rho A \\ \rho A u \\ \rho A(e + \frac{1}{2}u^2) \end{bmatrix} \tag{3}$$

and

$$\mathbf{F} = \begin{bmatrix} \rho A u \\ \rho A u^2 + pA \\ u[\rho A(e + \frac{1}{2}u^2) + p] \end{bmatrix}. \tag{4}$$

In this form, ρ is the fluid density, A is the area, u is the velocity, p is the pressure, and e is the specific internal energy. For problems of interest to blast modeling, the fluid is considered to be an ideal gas, for which the specific internal energy[7] is given by Equation 5.

$$e = \frac{p}{\rho(\gamma - 1)} \tag{5}$$

In this relationship, γ represents the ratio of specific heats and is assumed to be constant for the range of temperatures that are expected in shock tube applications.

3. SOLUTION METHOD

Time-accurate simulation of blast flow in air is accomplished here by first transforming the problem geometry into a computational domain where grid points may be uniformly or variably spaced along the length of the domain. The governing equations are discretized and then solved iteratively to march the solution through time. The MacCormack[8] finite difference scheme is used as the solution method. This explicit method uses a predictor-corrector approach for advancing the solution from the current time step to the next. In the predictor step, a forward difference is used to compute an interim solution at each grid point as illustrated in Equation 6.

$$q^*_{i,j} = q^n_{i,j} - \frac{\Delta t}{\Delta x_j}\left(F^n_{i,j+1} - F^n_{i,j}\right) \tag{6}$$

Here, the $q_{i,j}$ terms denote the conservation parameter from the vector of dependent variables, $\mathbf{q}$, from Equation 3, in which i represents the specific conservation parameter of mass, momentum and energy, and j represents the point in the grid at which the solution is being performed. Likewise, the $F_{i,j}$ and $F_{i,j+1}$ terms are used to identify the particular independent variable, i, at grid points j and $j+1$, respectively. The asterisk $(*)$ is used to identify the predicted conservation parameter and n is used to identify variables taken at the current point in time. The value of the time step is given by Δt, and Δx_j is the inter-grid spacing at grid point j.

After the predictor step is used to compute interim values of the $\mathbf{q}$ vector at every grid point, the corrector step uses the predicted values and a backward difference to compute the solution at the next time step for each grid point, as shown in Equation 7.

$$q^{n+1}_{i,j} = \frac{1}{2}\left[\left(q^n_{i,j} + q^*_{i,j}\right) - \frac{\Delta t}{\Delta x_j}\left(F^n_{i,j} - F^n_{i,j-1}\right)\right] \tag{7}$$

To account for area changes in the computational domain, the momentum equation, the second elements of Equations 3 and 4, is predicted in the manner shown in Equation 8.

$$q^*_{i,j} = q^n_{i,j} - \frac{\Delta t}{\Delta x_j}\left(F^n_{i,j+1} - F^n_{i,j} - p\frac{\Delta A_j}{\Delta x_j}\right) \tag{8}$$

And the corrector step takes the form

$$q_{i,j}^{n+1} = \frac{1}{2}\left[\left(q_{i,j}^{n} + q_{i,j}^{*}\right) - \frac{\Delta t}{\Delta x_j}\left(F_{i,j}^{n} - F_{i,j-1}^{n} - p\frac{\Delta A_j}{\Delta x_j}\right)\right]. \tag{9}$$

After the vector of dependent variables has been updated and the solution advanced in time, a new time step must be computed. The values of the **q** vector are used to compute the sound speed and the particle velocity at each grid point. The inter-grid spacing is then divided by the sum of the sound speed and the particle velocity to compute a signal propagation time for each grid point. The minimum signal propagation time in the grid is multiplied by a stability factor[9] which is less than 1.0 and the resulting value becomes the next time step. This method of computing the time step is summarized in Equation 10

$$\Delta t = CFL * MIN_j\left(\frac{\Delta x_j}{|u_j| + c_j}\right) \tag{10}$$

in which CFL is the stability factor, Δx_j is the grid spacing at grid point j, $|u_j|$ is the absolute value of the velocity at grid point j, and c_j is the sound speed at grid point j.

4. NORMAL SHOCK WAVES

Transient flow in shock tubes is characterized by the propagation of a shock front through undisturbed air. This leading shock may be followed by transient flow dictated by the geometry of the shock tube or other secondary shocks. In most shock tubes, the primary direction of flow is parallel to some reference axis. When the leading shock is perpendicular to the flow direction, it is referred to as a "normal shock wave." If the conditions of the undisturbed gas are known, then the conditions of the fluid immediately behind the normal shock can be completely described if only one parameter of the shock wave is known. This information can be used to compare a variety of fluid parameters from blast experiments to those values generated by a computational prediction, and this is useful in code validation efforts. The Rankine-Hugoniot Equations relate the gas parameters across the shock wave, and are derived from the conservation of kinetic energy between the states on either side of the shock.[10, 1]

The speed of the shock wave, the particle velocity behind the shock, and the density behind the shock are related to the pressure ratio across the shock by the relationships in Equations 11, 12, and 13. Here, p_∞, ρ_∞, and c_∞ are the ambient atmospheric pressure, density, and sound speed, respectively. The shock speed is represented by the symbol u_s, while the pressure, density, and velocity behind the shock are identified as p_1, ρ_1, and u_1, respectively.

$$\frac{u_s^2}{c_\infty^2} = \frac{1}{2\gamma}\left[(\gamma - 1) + (\gamma + 1)\frac{p_1}{p_\infty}\right] \tag{11}$$

$$\frac{u_1}{c_\infty} = \frac{1}{\gamma}\left(\frac{p_1}{p_\infty} - 1\right)\left[\frac{\gamma-1}{2\gamma}\frac{p_1}{p_\infty} + \frac{\gamma+1}{2\gamma}\right]^{-\frac{1}{2}} \tag{12}$$

$$\frac{\rho_1}{\rho_\infty} = \frac{(\gamma-1)\,p_\infty + (\gamma+1)\,p_1}{(\gamma+1)\,p_\infty + (\gamma-1)\,p_1} \tag{13}$$

5. BLAST FLOW MEASUREMENTS

Before presenting the comparison of shock tube experimental data with computational results, it is necessary to discuss the types of flow data that can be obtained in such experiments and how this information can be used to derive other fluid parameters. The primary means of collecting flow history data in shock tubes is through the use of pressure measurements. By measuring the static and stagnation overpressures at a point in the flow and knowing the ambient atmospheric conditions, it is possible to determine some useful information about the blast event. The dynamic pressure of a fluid in motion represents the kinetic energy per unit volume of the fluid and is a function of the fluid density and velocity. When the fluid being considered is an ideal gas, the dynamic pressure can also be expressed as a function of the pressure and the local Mach number which may be obtained from the Pitot Equations. For subsonic flow, the dynamic pressure, q, may be calculated from the static pressure, p, and the stagnation pressure, p_0, according to Equation 14.

$$q = \frac{\gamma}{2}\frac{2p}{\gamma-1}\left[\left(\frac{p_0}{p}\right)^{\frac{\gamma-1}{\gamma}} - 1\right] \tag{14}$$

For low speed subsonic blast flows, small errors or oscillations in the measured static and stagnation overpressure histories can lead to difficulty in accurately calculating the local Mach number and dynamic pressure behind these weak shocks. To reduce the error in calculating dynamic pressure in such flows, a differential pressure gauge[11] can be used. This device has a single pressure-sensing element that directly measures the difference between stagnation and static pressure. When a static gauge and a differential pressure gauge are used to measure the flow histories at a common point in the flow field, the two records may be summed to yield the stagnation pressure that can then be used to determine the local Mach number and dynamic pressure.

For cases in which the differential pressure gauge and the static pressure gauge are not close enough to justify summation to determine the stagnation overpressure, the measured differential pressure may be used to approximate the dynamic pressure. Figure 1 illustrates the relationship of differential pressure and dynamic pressure to local Mach number. For all the cases presented in this report, the local Mach number is less than 0.7. At this Mach number, the ratio of differential pressure to ambient static pressure is 0.38 and the ratio of dynamic pressure to ambient static pressure is 0.34. The relative difference between the differential pressure and dynamic pressure at this Mach number is 12%. This small relative

difference is evidence that the differential pressure can be reliably used to approximate the dynamic pressure for subsonic blast flows.

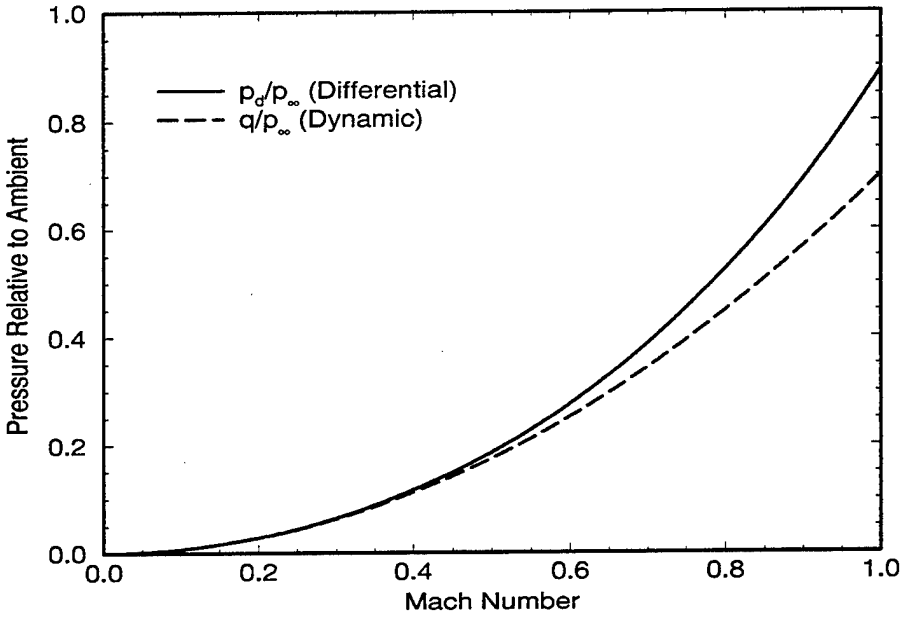

Figure 1. Differential and Dynamic Pressure as a Function of Shock Strength.

Having discussed the relationships between experimental flow measurements, it is necessary to develop a strategy which will be used in employing experimental data to derive other flow parameters and a set of rules for comparing experimental data to computed results. The following is the list of rules that are used to determine which flow parameters to compare with computational results:

1. If only one pressure gauge is used at a given location, its results will be directly compared to the simulation.
2. If any two different types of pressure gauges are used at a common location, the data recorded by those gauges will be used to derive the dynamic pressure and Mach number histories at that location. If static overpressure is not one of the measured histories, it will be derived from the measured data as well.
3. For locations that have at least two different types of gauges, the static overpressure, dynamic pressure, and Mach number histories will be compared to the simulation.
4. For locations that have only one type of gauge, that information will be compared with the simulation.

6. SINGLE STAGE SHOCK TUBE FLOW SIMULATIONS

The intended use of the flow solver described in this report is the numerical simulation of time-dependent flow in shock tubes and blast simulators. This type of analytical tool can be used to study possible shock tube configurations so that particular flow patterns can be produced, experiments can be designed for blast simulators, predicted environments can be predicted for gauge ranging in blast tests, or 1-D blast wave histories can be generated for use as an inlet boundary condition for a separate numerical simulation.

To validate the code for modeling the types of flow fields encountered in shock tube experiments, shock tubes of various configurations were selected and calculations were performed to match experiments from each facility. These validation cases are presented in order of increasing geometric complexity.

6.1. Constant Area Shock Tube

The simplest shock tube geometry is that of a straight tunnel with constant cross-sectional area. One such facility is the 57-cm shock tube at ARL.[12] This shock tube consists of a cylindrical driver tube and expansion section, a square section, and an additional cylindrical expansion region down stream from the test section. The cylindrical tube sections are 57.47 cm in diameter, and the square test section is 50.80 cm on a side to yield a constant cross-sectional area of 0.26 m^2. The length of the driver section is adjustable from 30.48 cm to 16.76 m. The distance from the beginning of the expansion tunnel to the measurement station is 30.48 m.

A calculation was performed to model a test of this facility in which the driver length was 91.44 cm, the driver overpressure was 379.2 kPa, The ambient pressure was 102.1 kPa, and the ambient temperature was 294.5 K. The driver gas was supplied by air compressors and the pressurized air was at the same temperature as the surrounding atmosphere. The calculation was performed using a computational domain which was discretized with a uniform grid spacing of 4 cm. The static overpressure, dynamic pressure, and Mach number histories produced by the simulation are compared to the measured data in Figures 2 through 4, and Table 1 provides a summary the comparison between the experiment and the calculation.

The static overpressure comparison shows some oscillation in the computed history immediately after the shock arrives at the measurement position. After this period of oscillation, which lasts about 2 ms, the computed history follows the experimental data to within 2 kPa. These characteristics of initial oscillation after the shock arrival, followed by close agreement with the experimental data are evident in the dynamic pressure and Mach number histories as well.

The oscillations occurring near the shock arrival are the result of dispersion—the numerical propagation of plane waves through the computational domain.[13] The presence of these oscillations makes it difficult to determine the amplitude of the incident shock in time-dependent flow histories such as those shown in Figures 2 and 3. However, the pressure

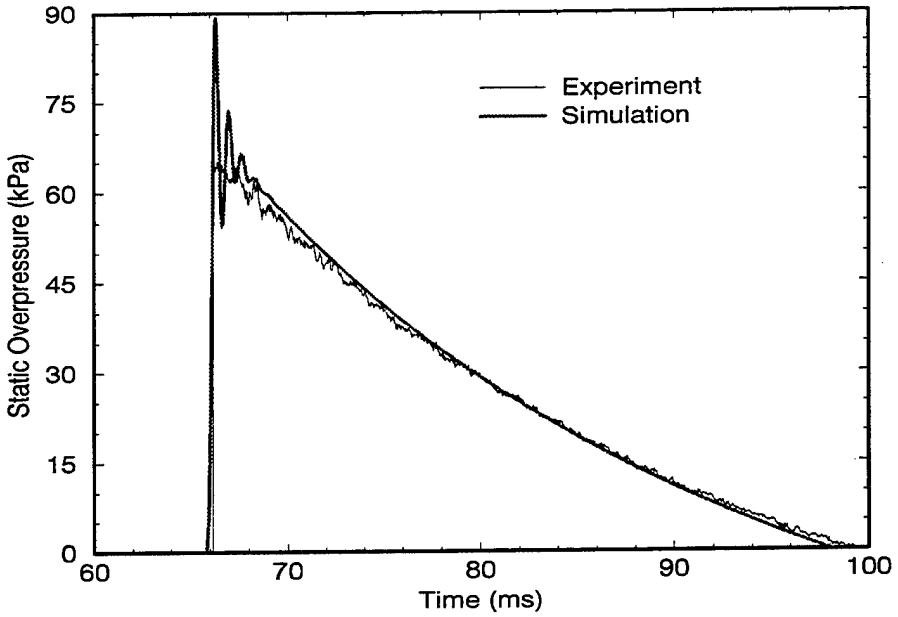

Figure 2. 57-cm Shock Tube Test: Static Overpressure.

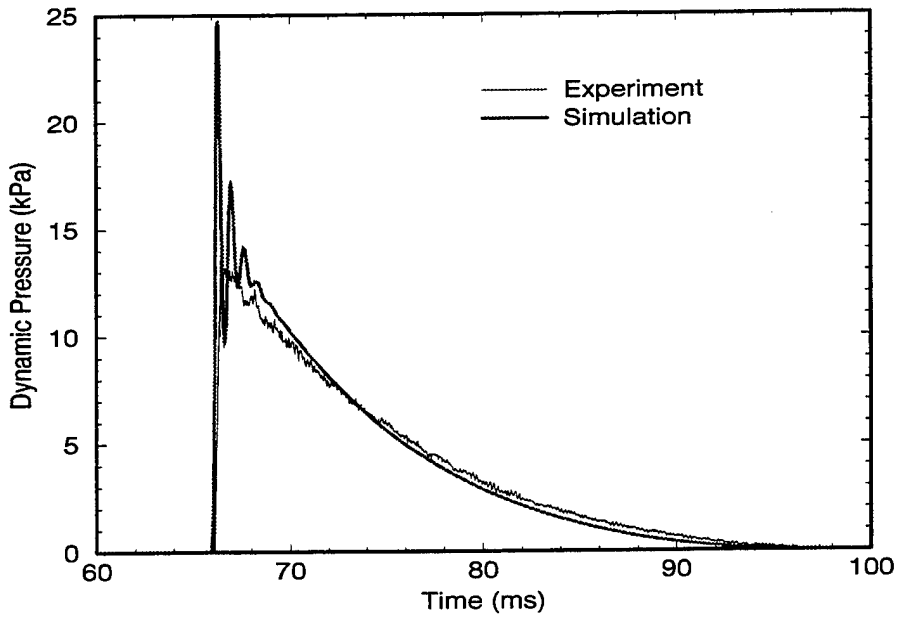

Figure 3. 57-cm Shock Tube Test: Dynamic Pressure.

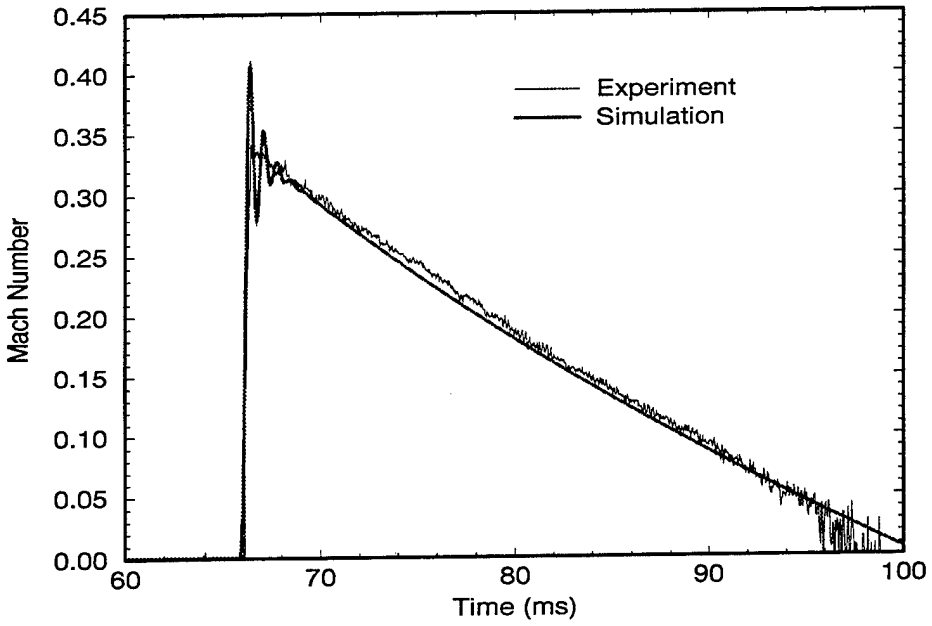

Figure 4. 57-cm Shock Tube Test: Mach Number.

immediately behind the shock can be determined from the computed speed of the shock wave. By placing additional monitoring stations in the computational domain in the vicinity of the target location, the shock wave speed may be determined by observing the difference in shock arrival times at the different positions. For this calculation, the shock wave speed was found to be 436.7 m/s. Using the Rankine-Hugoniot equations described earlier, the incident shock overpressure computed by the code is found to be 71.2 kPa, 7.4% greater than the measured overpressure. The dynamic pressure and local Mach number behind the incident shock were similarly over-predicted by the computation.

Table 1. Summary of Results for 57-cm Shock Tube Test.

	Experiment	Simulation	Error
Shock Wave Speed	-	464 m/s	-
Incident Static Overpressure	66.3 kPa	71.2 kPa	+7.4%
Dynamic Pressure Behind Shock	13.6 kPa	16.6 kPa	+22.1%
Mach Number Behind Shock	0.34	0.37	+8.8%
Static Overpressure Impulse at 100 ms	0.88 kPa-s	0.90 kPa-s	+2.3%
Dynamic Pressure Impulse at 100 ms	0.122 kPa-s	0.125 kPa-s	+2.5%

6.2. Variable Area Shock Tube

The next level of geometric complexity to be studied in the validation of the code is that of a shock tube with a varying cross-sectional area. One such facility is the ARL 2.44-m blast simulator,[15] a schematic diagram of which is presented in Figure 5. This facility has a cylindrical driver 91.44 cm in diameter and 9.42 m in length. A converging nozzle, located at the downstream end of the driver, channels the flow into a throat section which is half the diameter of the driver section. Two diaphragms om the throat section initially separate the

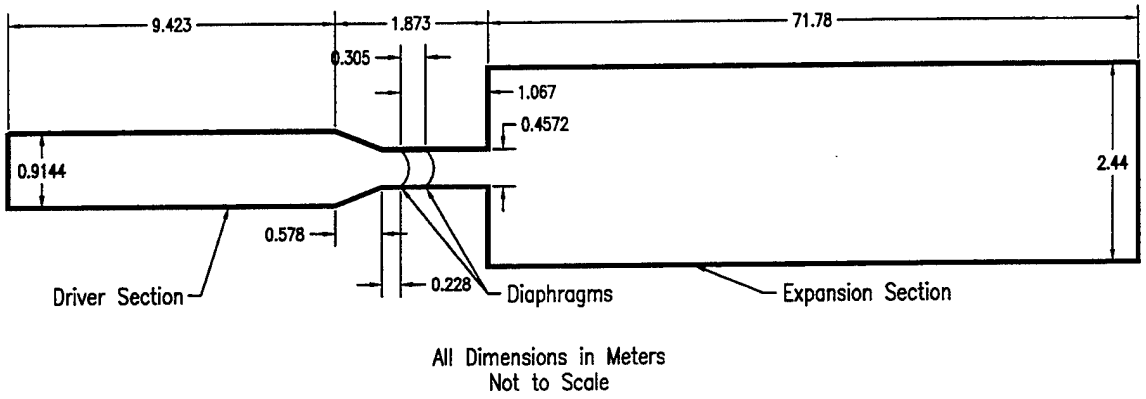

Figure 5. 2.44-m Blast Simulator Schematic Diagram.

high pressure driver gas from the ambient air. Before a test, the pressure is increased from ambient to the high pressure driver condition by incremental pressure increases across the diaphragms. The net pressure difference from the driver condition to the ambient state is greater than either of the diaphragms can maintain, but the pressure differential across either of the diaphragms is less than the rupture pressure of the diaphragms. Flow is initiated by releasing the gas between the two diaphragms, causing the upstream diaphragm to rupture first, followed by the downstream diaphragm. At the downstream end of the throat, there is an immediate transition to the expansion tunnel, which is 2.44 m in diameter and 71.78 m in length. Static overpressure and differential pressure histories are recorded in the expansion section at a position 15.86 m down stream from the beginning of the expansion section.

There are two significant differences between the computational model of the 2.44-m blast simulator and the actual facility. As stated earlier, the momentum calculation in the MacCormack predictor-corrector technique contains an additional term to account for the rate of area change per unit length in the computational domain. In the case of the 2.44-m blast simulator, the immediate area change at the throat exit produces in an infinite rate of area change per unit length. As a result, this abrupt area change cannot be incorporated into the computational domain. To simulate the flow in this facility, an artificial diverging nozzle with a 30° half angle was used to transition from the outer radius of the throat section to the outer radius of the expansion section, thereby providing a finite rate of area change per unit length throughout the computational domain.

The second significant difference between the 2.44-m blast simulator and its corresponding computational model is the method used to specify the initial conditions. As stated

earlier, the high pressure driver gas and the ambient air are separated by two diaphragms that have an intermediate pressure level in between them. In the computational model, the downstream diaphragm and the fluid at the intermediate pressure state are completely ignored. Instead, the computational domain is initialized with the driver gas and the ambient air immediately adjacent to each other at a grid point corresponding to the position of the upstream diaphragm.

The model of the 2.44-m blast simulator was discretized with a uniform grid spacing of 10 cm. A calculation was performed to simulate a test that had been conducted in this facility. The test was performed with an ambient pressure of 101.5 kPa, an ambient temperature of 313.7 K, a driver overpressure of 5.21 MPa, and driver temperature of 354 K. The flow histories derived from the experimental data are compared to the computed histories in Figures 6 through 8 and summarized in Table 2.

Table 2. Summary of Results for 2.44-m Blast Simulator Test.

	Experiment	Simulation	Error
Shock Wave Speed	-	480 m/s	-
Incident Static Overpressure	100.8 kPa	96.6 kPa	-4.2%
Dynamic Pressure Behind Shock	31.3 kPa	28.9 kPa	-7.7%
Mach Number Behind Shock	0.47	0.46	-2.1%
Static Overpressure Impulse at 300 ms	12.9 kPa-s	12.1 kPa-s	-6.2%
Dynamic Pressure Impulse at 300 ms	2.08 kPa-s	2.39 kPa-s	+14.9%

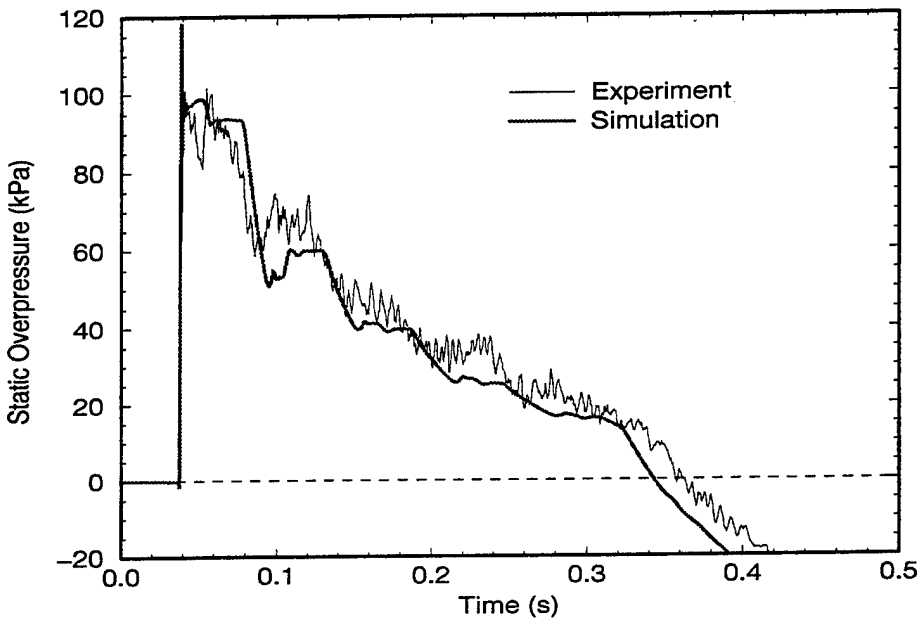

Figure 6. 2.44-m Blast Simulator Test: Static Overpressure.

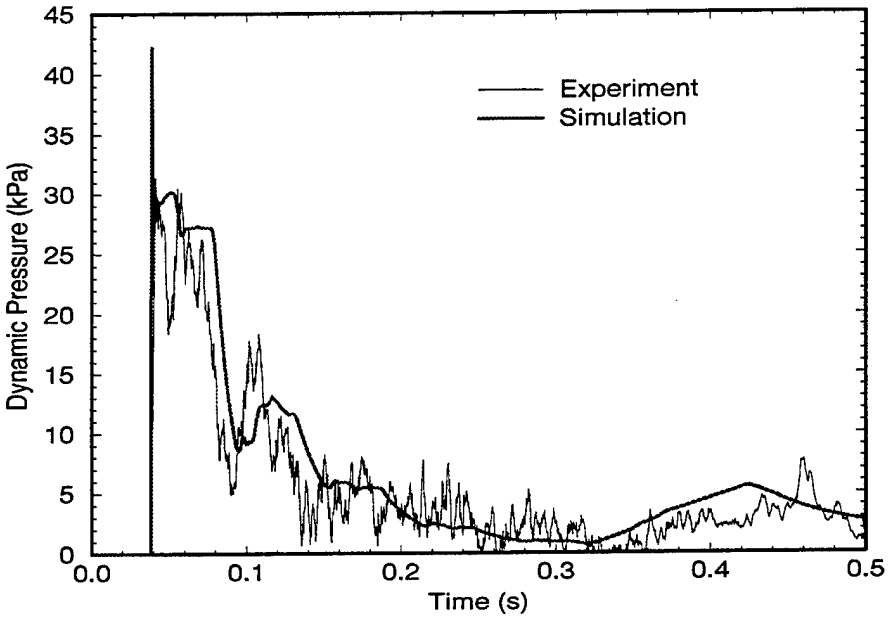

Figure 7. 2.44-m Blast Simulator Test: Dynamic Pressure.

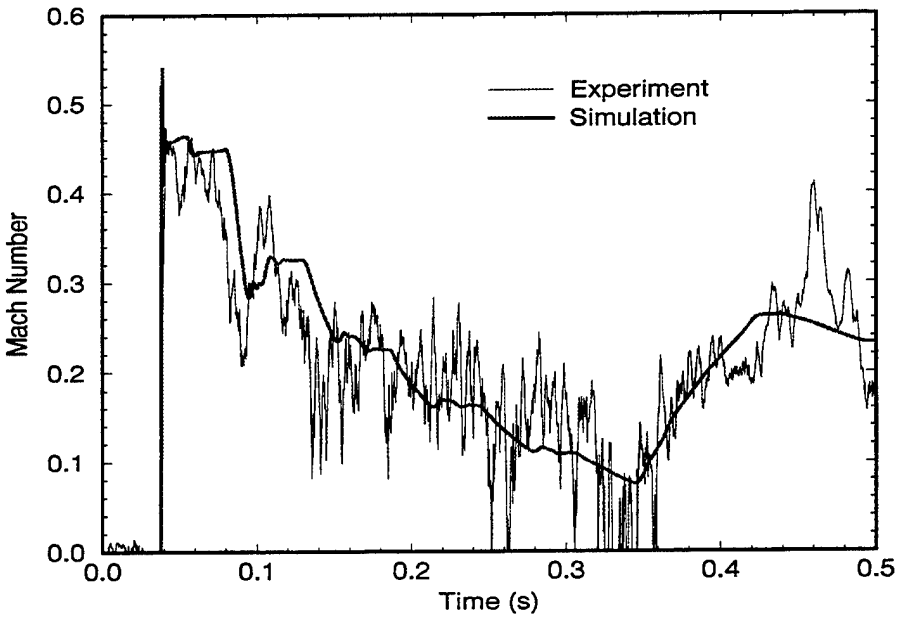

Figure 8. 2.44-m Blast Simulator Test: Mach Number.

The static overpressure histories are provided in Figure 6 and illustrate the experimental peak static overpressure of 100.8 kPa. The shock wave speed in the simulation of this experiment was 480 m/s. Using the Rankine-Hugoniot relation from Equation 11, the peak static overpressure from the calculation was determined to be 96.6 kPa, under-predicting the experimental peak by 4.2%. From the time of shock arrival to about 350 ms, the computational static overpressure history and dynamic pressure history of Figure 7 exhibit a "stair step" decay pattern. These distinct decreases in the flow histories signify the passage of expansion waves originating from the driver tube. This same decay pattern can be seen in the experimental data in the two figures and compare well with the computed histories.

In shock tube tests such as the one described here, when the primary shock reaches the downstream end of the expansion section, it encounters the sudden area change at the tunnel exit. No longer contained by the walls of the expansion section, the shock expands rapidly into the surrounding atmosphere. The sudden expansion of the shocked gas causes a rarefaction wave to form at the tunnel exit. This rarefaction wave travels up stream against the direction of fluid flow. The pressure on the downstream side of the rarefaction wave is lower than the pressure on the upstream side. As the rarefaction wave propagates up stream, the fluid particles that were set in motion by the primary shock encounter the reduced pressure on the downstream side of the rarefaction wave and are accelerated. The code is able to simulate the generation of the rarefaction wave through the use of an inflow-outflow boundary condition at the downstream end of the computational domain. This boundary condition forces the thermodynamic pressure at the outlet to be always equal to the reference atmospheric pressure. In Figure 6, the static overpressure decreases suddenly at a time of about 350 ms corresponding to the arrival of the rarefaction wave at the measurement position. At this same time, the dynamic pressure (see Figure 7) and Mach number (see Figure 8) are observed to increase as a result of the acceleration of the shocked gas by the passage of the rarefaction wave. The use of the inflow-outflow boundary condition at the downstream end of the computational domain allows the code to simulate the formation and propagation of the rarefaction wave as evidenced by the agreement between the experimental and computed histories after the arrival of the rarefaction wave at the test station.

The experimental and computational static overpressures were integrated to determine the static overpressure impulse and the differential pressure impulse. At 300 ms, the static overpressure impulse of the experimental data has reached a value of 12.9 kPa-s, while the impulse from the computational history was 12.1 kPa-s, a difference of 6.2%. In the case of the differential pressure, the impulse of the experimental history at 300 ms is 2.13 kPa-s, while that of the simulation is 2.48 kPa-s, an over-prediction of 16.4%.

6.3. Variable Area Multiple Driver Blast Simulator

The shock tube geometries presented until now have been relatively simple in their configurations, with a central flow regime of either constant or variable cross-sectional area. The last level of geometric complexity to be studied in the validation of the code is that in which multiple driver tubes feed into a single expansion section. Such facilities have been used in France, Germany, and the United States to simulate exponentially decaying blast

flows associated with the detonation of tactical nuclear weapons.[5] These multi-driver blast simulators typically use driver tubes of assorted lengths. When the driver tubes are charged to a uniform initial state and fired simultaneously, the driver tubes produce expansion waves at different frequencies. This approach helps to eliminate the "stair step" pattern of the pressure histories, allowing them to be more like an exponential decay.

To model the flow in multi-driver shock tubes with the code, the actual 3-D geometry of such a facility must be reduced to a domain with one computational dimension that has area changes along that dimension. This is accomplished by combining the total available flow area into an equivalent cross-sectional area at every point along the length of the facility. Using this technique, the 1-D computational model contains the same total volume, mass, energy, and relative area changes of the actual facility and would be expected to produce adequate results for longitudinal positions in the facility where the flow is expected to be nearly uniform across the entire cross section. However, the simplification of the geometry into this 1-D form makes it impossible to properly study the flow where there is significant mixing of the gas exiting the different driver tubes.

One example of a multi-driver shock tube is the Large Blast/Thermal Simulator (LB/TS), at the White Sands Missile Range in New Mexico, and operated under the direction of the Defense Special Weapons Agency (DSWA). A photograph of this facility is provided in Figure 9. The LB/TS has nine cylindrical driver tubes, each with a diameter of 1.83 m. These tubes can be seen near the lower right corner of the photograph. At the downstream end of each driver tube is a converging nozzle 1.45 m in length. The nozzle transitions the available cross section from the driver diameter of 1.83 m to the throat diameter to 0.91 m. In the throat section, the distance from the downstream end of the converging nozzle to the diaphragm is 1.63 m, and the distance from the diaphragm to the downstream end of the throat section is 2.29 m.

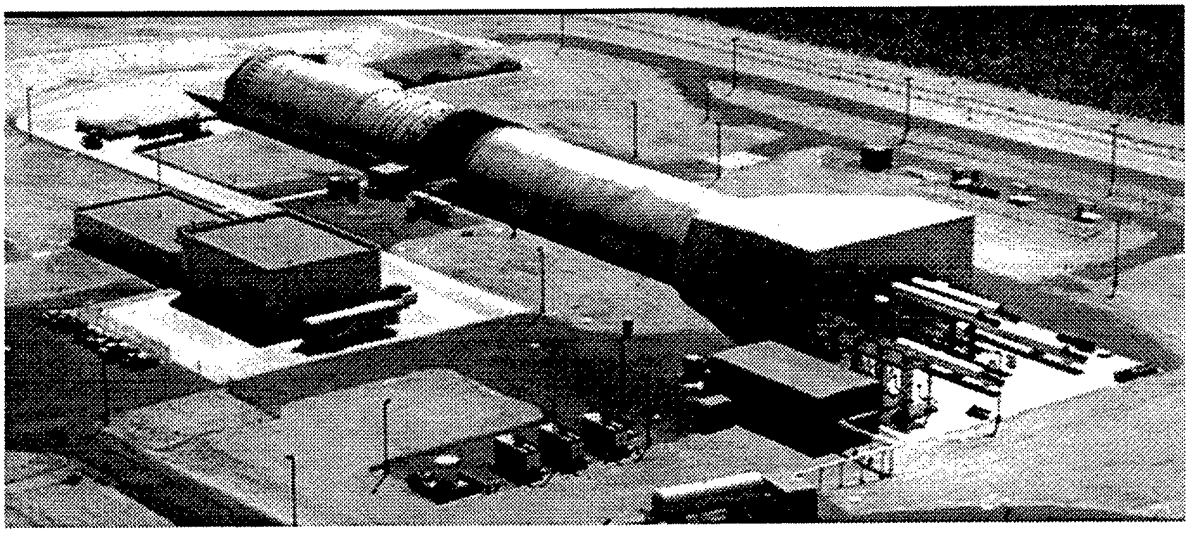

Figure 9. Large Blast/Thermal Simulator.

The lengths of each of the cylindrical driver tubes can be adjusted by securing a special plug inside each tube before a test. With these plugs placed so that the maximum driver lengths are obtained, the lengths of the cylindrical driver tubes are as follow:

- two tubes, each 11.0 m long,
- three tubes, each 19.9 m long,
- two tubes, each 28.4 m long, and
- two tubes, each 36.2 m long.

The expansion section is 170 m long and is in the shape of a horizontal semi-cylinder with a cross-sectional area of 163 m^2. The upstream end of the expansion section is a vertical wall, with the downstream ends of the nine throat sections flush with the wall. At the downstream end of the expansion section is a rarefaction wave eliminator[16] (RWE). The RWE can make the expansion tunnel appear to be infinitely long as it suppresses the formation of an expansion wave when the shocked air exits the expansion section. The RWE is mounted on railroad tracks so that it can be moved to the side to provide equipment access to the interior of the expansion section.

A calculation was performed to model the LB/TS for a test in which the nine driver tubes had been configured at their maximum volume. The initial overpressure of the gas in the driver tubes was 3.44 MPa and the initial temperature of the driver gas was 414 K. The ambient pressure and temperature used for the calculation were 84.9 kPa and 288.7 K, respectively. The geometry of the upstream end of the computational model is illustrated in Figure 10. The model was developed using the area combination method described earlier and the domain was discretized with a uniform grid spacing of 40 cm. As in the case with the 2.44-m blast simulator, an artificial diverging nozzle was used in the computational model to transition the area from the exit of the throat sections to the area of the expansion section. In this case, a diverging nozzle half-angle of 45^o was used.

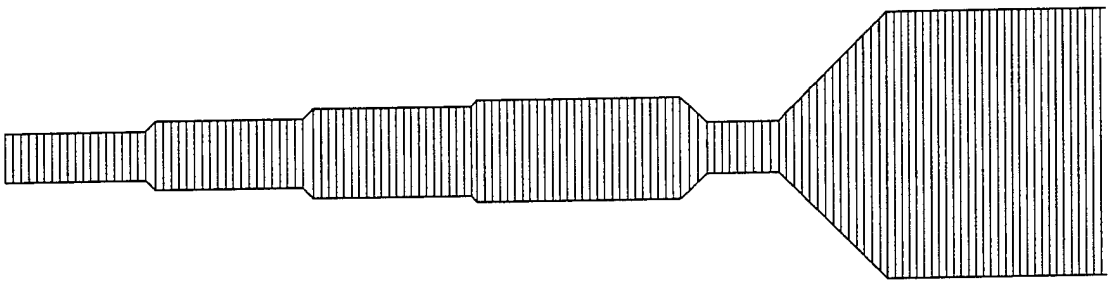

Figure 10. LB/TS Model for Single Stage Test: Upstream End.

In this single stage experiment, the RWE was used to minimize flow disturbances that would be created by the sudden expansion of the shocked gas at the exit plane of the expansion section. The influence of the RWE on the exit flow is replicated in the calculation through the use of the inflow/outflow boundary condition described earlier and changes in the grid geometry as a function of time. A converging nozzle is placed at the downstream

end of the computational domain and the exit area is changed with time so that it matches the exit area history of the RWE in the experiment. The variation in grid geometry at the downstream end is illustrated in Figure 11. This figure shows the different exit areas at times of 0.0, 0.6, 1.0, and 1.4 s. The exit area is held constant from the beginning of the calculation until the arrival of the shock at the exit plane at about 0.36 s. After then, it is decreased during the event to accelerate the flow and reduce the effect of the short tunnel on the flow at the test section.

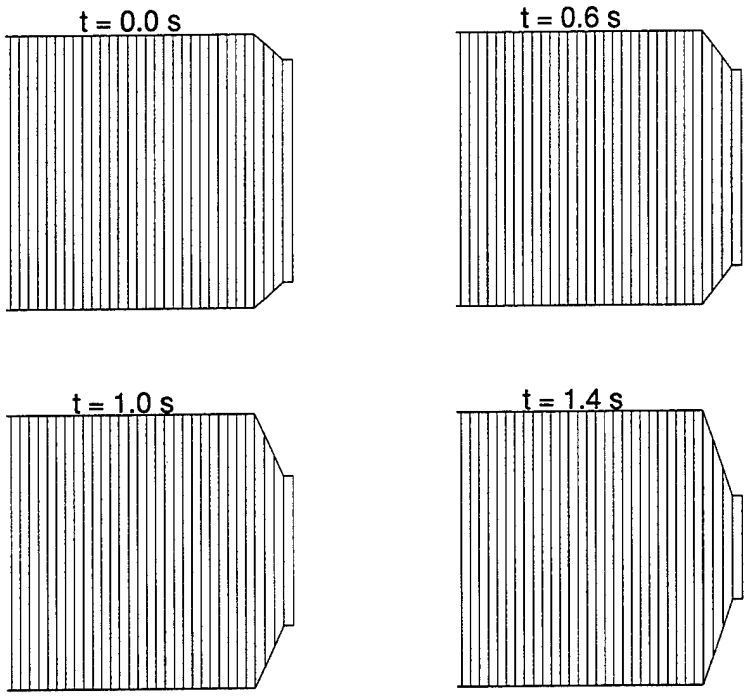

Figure 11. LB/TS Model for Single Stage Test: Downstream End.

The LB/TS is configured so that instrumentation may be placed at a number of positions throughout the expansion section for measuring blast histories. For the purpose of code validation, comparisons were made using data collected at a position which is 105 m from the upstream end of the expansion section. This corresponds to the typical location of equipment that is placed in the expansion tunnel for blast testing. The computed histories from this test station are compared to the experimental data in Figures 12 through 14. The computational and experimental data are also summarized in Table 3. Figure 12 shows a peak static overpressure from the experiment of 80.8 kPa while that of the simulation was 75.9 kPa. The static overpressure positive phase ends at approximately 750 ms, at which time the impulse was 20.4 kPa-s for the calculation, over-predicting the experimental value of 18.8 kPa-s by 8.5%.

At a time of approximately 650 ms in Figure 12, there is a spike in the computed static overpressure history, followed by a sudden decrease in the static overpressure of both the experimental and computed histories. At this same time in the dynamic pressure histories (see Figure 13), there is an increase. This is an indication that the open area at the

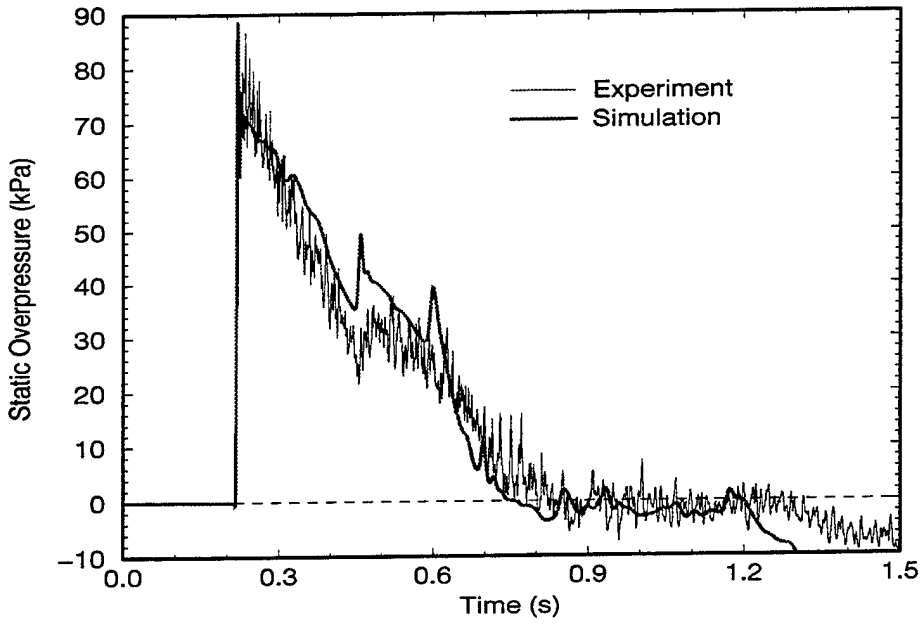

Figure 12. LB/TS Single Stage Test: Static Overpressure.

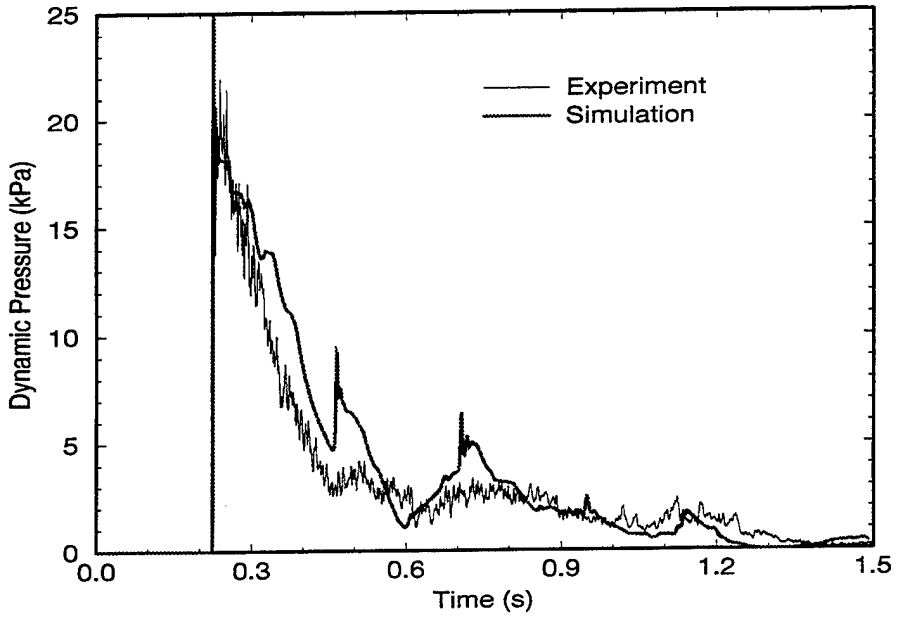

Figure 13. LB/TS Single Stage Test: Dynamic Pressure.

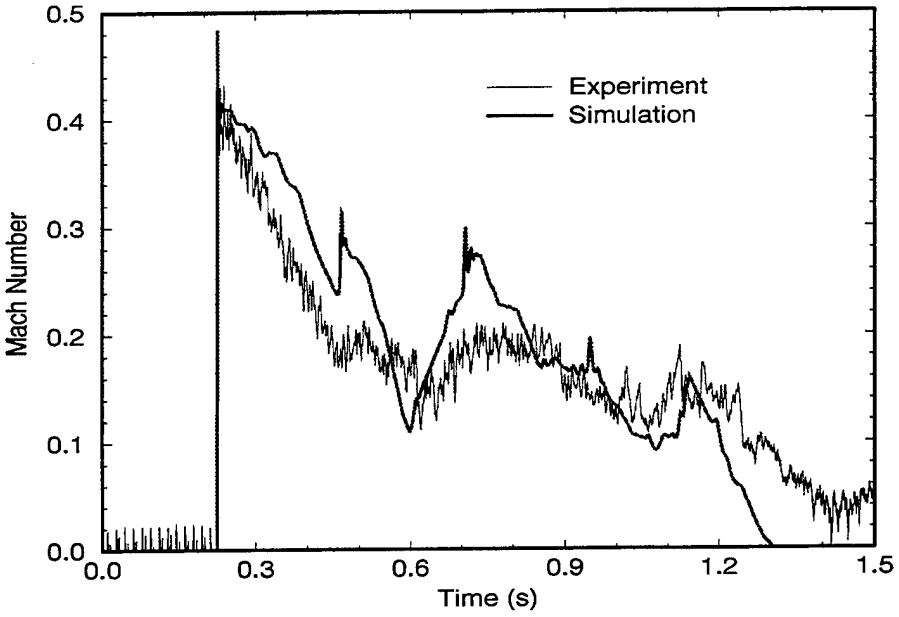

Figure 14. LB/TS Single Stage Test: Mach Number.

downstream end of the expansion tunnel was not sufficiently decreased to fully eliminate the formation of an expansion wave. This resulted in the formation of a weak expansion wave at the downstream end of the expansion section that propagated up stream and caused a slight increase in the particle velocity, resulting in the pressure drop and dynamic pressure increase evident the the figures. The increase in particle velocity beginning at 650 ms is also evident in the Mach number history of Figure 14. The simulation properly predicts the effect of the expansion wave on the Mach number and dynamic pressure histories but over-predicts its magnitude. After the arrival of the expansion wave, the simulated Mach number history reaches a maximum of 0.30 at 700 ms, while the experimental result increases to only 0.21. At the same times the simulated dynamic pressure increases to 6.35 kPa while the experiment increases to 3.38 kPa.

Table 3. Summary of Results for LB/TS Single Stage Test.

	Experiment	Simulation	Error
Shock Wave Speed	-	455 m/s	-
Incident Static Overpressure	80.3 kPa	77.3 kPa	-3.7%
Dynamic Pressure Behind Shock	23.9 kPa	22.2 kPa	-7.1%
Mach Number Behind Shock	0.45	0.44	-2.2%
Static Overpressure Impulse at 750 ms	18.8 kPa-s	20.4 kPa-s	+8.5%
Dynamic Pressure Impulse at 1.0 s	4.16 kPa-s	4.81 kPa-s	+15.6%

Before the arrival of the weak expansion wave at the measurement position, the computed dynamic pressure history is consistently greater than the measured data from 300 ms to 650 ms. As a result of this and the over-prediction of the increased particle velocity from the weak expansion wave, the computed dynamic pressure impulse at 1.5 s was 15.6% greater than that obtained from the experiment.

7. MULTIPLE STAGE SHOCK TUBE FLOW SIMULATIONS

Recently, a need has arisen to generate complex blast flow histories in shock tubes. The most significant characteristics of these flow histories are the high levels of dynamic pressure and the presence of more than one dynamic pressure peak in the event.[17] For blast simulators with multiple, high pressure driver tubes, one way to accomplish this is to use a staged opening of the driver tubes. Using this technique, a shock generated by the opening of a set of drivers can be used to reinforce or diminish the presence of a particular flow pattern from a set of driver tubes opened previously. Flow fields of this type can be simulated using 2-D and 3-D CFD codes, but the computational analysis that is required can be very time consuming as the simulation of one multi-stage test may actually consist of several calculations that provide information to each other. To decrease the time spent in designing a multi-stage shock tube test, the capability to model this type of event was added to the code. This 1-D modeling capability allows the analyst to study a range of possible test conditions in a short period of time. This analysis would eliminate the cases that have little chance of success and allow the analyst to perform more detailed 2-D or 3-D computations for those cases that have a greater chance of success.

Because the code solves the equations of motion in only one dimension, it is not possible for a single computational model to replicate the individual driver tubes firing at different times. To make the simulation possible, separate calculations are performed to model the exit flow from the banks of driver tubes for each individual stage of a multi-stage event. For each of these independent calculations, the primitive flow parameters (pressure, density, and velocity) are collected as a function of time at the driver exit. The driver exit history data are then processed and used as an inlet boundary condition for a separate simulation of the multi-stage event.

Since only one computational dimension exists, the multiple driver exit histories may not be used independently to drive the simulation of the multi-stage flow. The histories must be combined and provided as a single flow history. Conservation laws are used to provide a basis for combining the multiple histories into a single history of primitive flow variables and inlet area. Specifically, the total mass, momentum, energy, and inlet cross-sectional area are conserved in the combined history as defined in Equations 15 and 16.

$$(q_i)_{net} = \sum_{m=1}^{n} (q_i)_m \tag{15}$$

$$A_{net} = \sum_{m=1}^{n} A_m \tag{16}$$

In these equations, q_i represents the conservation parameter of mass, momentum, or energy, and A represents the driver exit area. The summation of m from 1 to n is used to denote the number of active inlet histories at the point in time when the calculation is performed. The summations produce the combined inlet flow history denoted with the *net* subscript.

After the total mass, momentum, energy, and inlet cross-sectional area are computed, the net density is computed by dividing the total area into the net mass term as in Equation 17:

$$\rho_{net} = \frac{\sum_{i=1}^{n} \rho_i A_i}{\sum_{i=1}^{n} A_i} \tag{17}$$

The net velocity is computed by dividing the mass term into the momentum term as illustrated in Equation 18:

$$u_{net} = \frac{\sum_{i=1}^{n} \rho_i u_i A_i}{\sum_{i=1}^{n} \rho_i A_i} \tag{18}$$

From Equations 3, 5, and 15, the total energy from the individual histories is given by Equation 19:

$$\left[A\left(\frac{p}{\gamma-1}+\frac{1}{2}\rho u^2\right)\right]_{net} = \sum_{i=1}^{n}\left[A_i\left(\frac{p_i}{\gamma-1}+\frac{1}{2}\rho_i u_i^2\right)\right] \tag{19}$$

Using the net area, density and velocity from the previous equations, Equation 19 can be solved for the net pressure as shown in Equation 20:

$$p_{net} = (\gamma-1)\left[\frac{1}{A_{net}}\sum_{i=1}^{n}\left(\frac{p_i}{\gamma-1}+\frac{1}{2}\rho_i u_i^2\right)A_i - \frac{1}{2}\rho_{net}u_{net}^2\right] \tag{20}$$

Performing this set of calculations produces the history of net pressure, density, and velocity which is used as a time-dependent, inlet boundary condition for the multi-staged simulation.

7.1. Two-Stage Tests

Generation of high dynamic pressure flows with a two-stage driver firing sequence is accomplished by first releasing the gas from a specified bank of drivers. When the leading shock from this first bank reaches the downstream end of the expansion section, a rarefaction wave is formed, which travels up stream in the expansion section, accelerating the shocked gas as it propagates up stream. The timing of flow initiation from the second driver bank is such that the shock formed by the second driver release arrives at the desired location at the same time as the rarefaction wave. This coincidental arrival of the second shock and the rarefaction wave produces a sudden increase in the dynamic pressure.

Two tests of this type have been performed in the LB/TS. The RWE was not used in either test. In both cases, the first bank of drivers was comprised of the five longest individual driver tubes, having a combined total volume 385 m^3. The second bank was comprised of the four shortest driver tubes with a total volume of 168 m^3. Releasing the large bank first forces the majority of the driver gas into the expansion tunnel early in the event. The purpose of the second bank is to propagate a shock behind the driver gas released by the first bank and drive it down the tunnel.

Simulation of a two-stage test is accomplished through the setup and execution of three separate calculations. The first calculation simulates the independent firing of the first bank of driver tubes into the expansion section. The same is done for the second bank in a separate calculation. In each of these two calculations, the flow histories are recorded at the downstream end of the throat section, where the driver gas flows into the expansion section. These two, independent flow histories are then combined using the methodology described earlier in this section to produce a single representative history of pressure, density, velocity, and inlet area.

The final calculation is designed to simulate only that portion of the shock tube down stream from the throat section. At the upstream end of this computational model, the area is varied with time to simulate the increase in available flow area when the second driver bank is released. The combined history from the individual driver calculations is supplied as a forcing function at the upstream boundary.

In the first of these two-stage tests, the bank of five drivers was charged to an overpressure of 2.96 MPa and a temperature of 310.9 K, while the bank of four drivers was initialized with an overpressure and temperature of 6.41 MPa and 449.8 K, respectively. When the test was performed, one of the diaphragms in the five-driver bank failed to open, leaving only four tubes to drive the first pulse. The second driver bank was fired 300 ms after the first.

To simulate this test, the computational model of the first driver bank consisted only of the four driver tubes that opened. The model of the second driver bank was also developed using the area combination method described earlier. These two calculations were performed and the flow histories at the throat exit were used to generate the inlet history for the staged flow calculation. In the staged flow calculation, the inlet area was varied with time to model the changing available flow area as the drivers are opened. From a time of zero to 300 ms, the inlet cross-sectional area was 2.63 m^2, corresponding to the area of the four active drivers in the first bank. At 300 ms, the inlet area was immediately doubled to account for the additional four drivers in the second bank, then held constant for the remainder of the simulation. Figure 15 shows the pressure, density, and velocity histories of the inlet flow. In these figures, a time of zero corresponds to the time of diaphragm rupture of the first driver bank. Immediately after the diaphragm rupture of the first bank, the pressure, density, and velocity increase and then begin to decay gradually. At 300 ms, the inlet area is immediately opened to the equivalent cross-sectional area of all eight throat sections, causing the sharp drop in the inlet histories. Immediately after this increase in inlet area, the flow from the second driver bank is initialized and the flow parameters again increase suddenly, then slowly decay as the driver tubes empty.

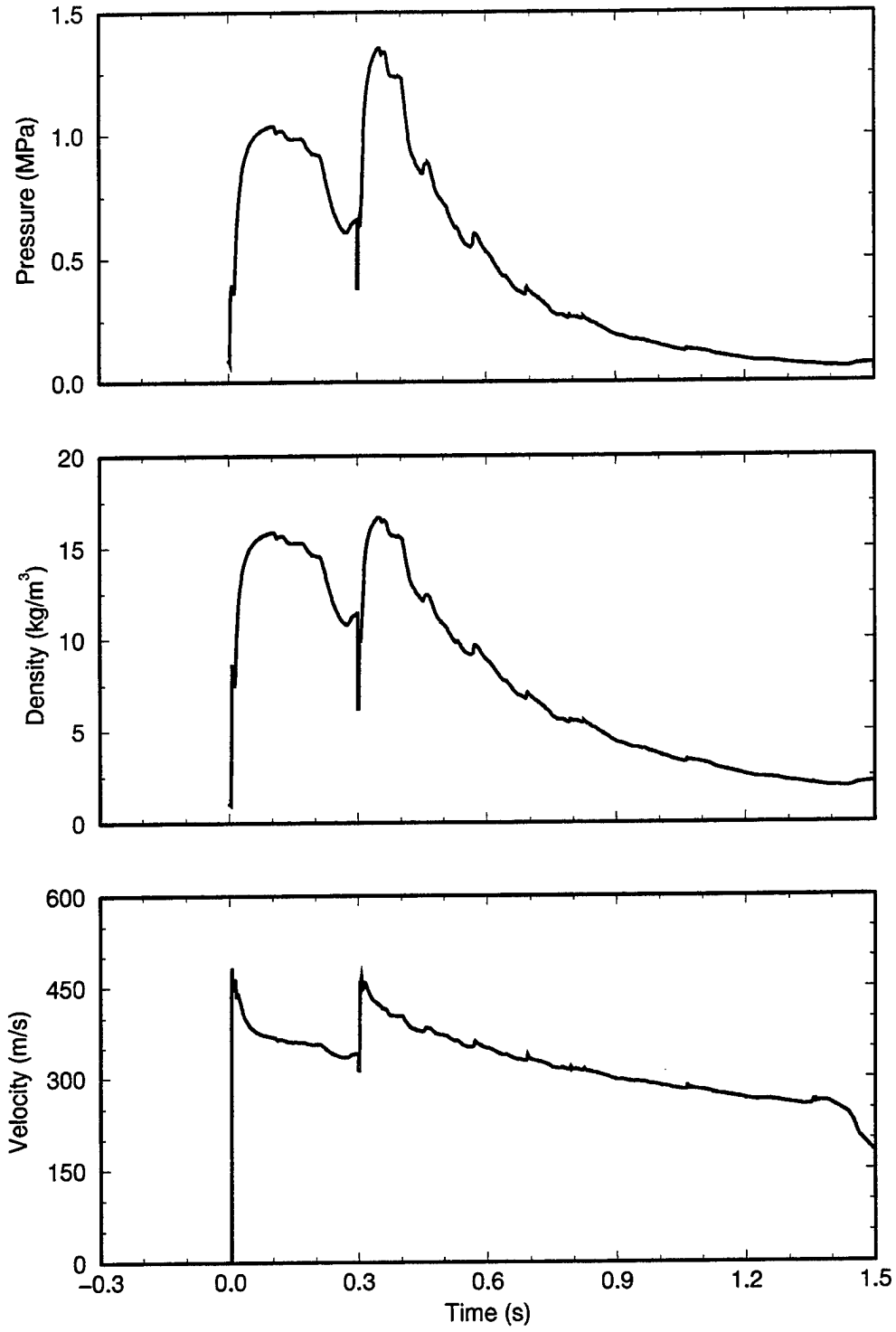

Figure 15. LB/TS Two-Stage Test #1: Inlet Histories.

A static overpressure history was recorded at a position 103.8 m from the upstream end of the expansion tunnel, stagnation pressure measurements were recorded at 105.8 m and 141.1 m, and differential pressure data were collected at 141.2 m. The conditions behind the first shock and the impulse values for the experimental and computed histories are provided in Table 4. The static overpressure data are plotted in Figure 16 and the stagnation overpressure history data from the gauge at 105.8 m are shown in Figure 17. These figures show the arrival of the first shock at 260 ms, and the arrival of the second shock at 520 ms. The calculation under-predicts the amplitude of both the incident static overpressure and the incident stagnation pressure. The arrival of the rarefaction wave at the 103.8-m location is visible in both the experimental and computed static overpressure histories at approximately 700 ms, where the downward slopes of the curves increase and lead to the the end of the positive phase of the event at approximately 800 ms.

Table 4. Summary of Results for LB/TS Two-Stage Test #1.

	Experiment	Simulation	Error
Shock Wave Speed	-	395 m/s	-
Incident Static Overpressure	40.9 kPa	34.2 kPa	-16.4%
Dynamic Pressure Behind Shock	6.6 kPa	4.7 kPa	-28.8%
Mach Number Behind Shock	0.27	0.24	-11.1%
Static Overpressure Impulse at 800 ms (103.8 m)	17.7 kPa-s	17.0 kPa-s	-4.0%
Static Overpressure Impulse at 900 ms (141 m)	11.0 kPa-s	9.0 kPa-s	-18.2%
Dynamic Pressure Impulse at 1.3 s (141 m)	8.0 kPa-s	8.7 kPa-s	+8.8%

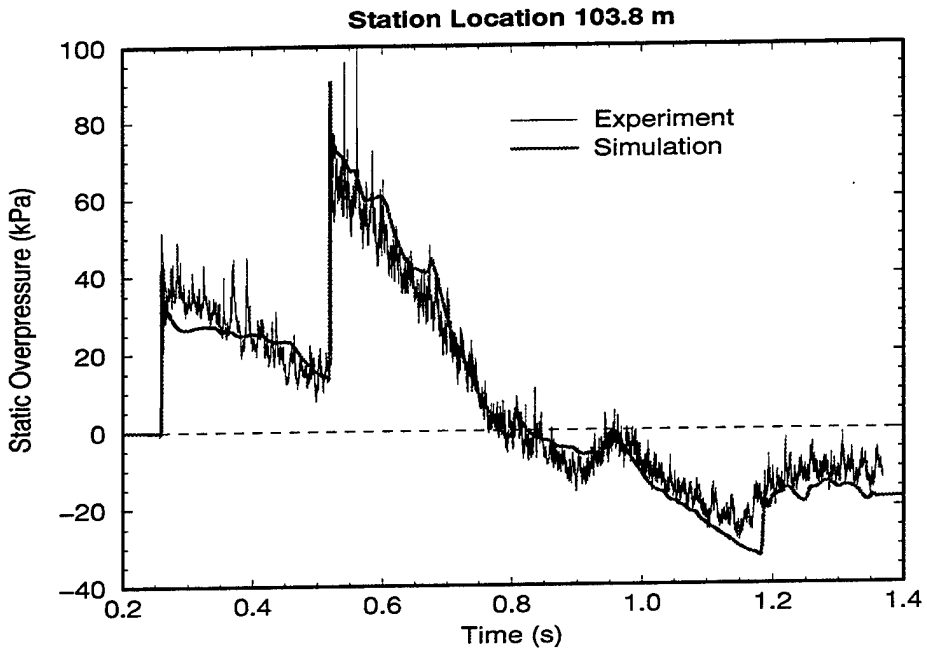

Figure 16. LB/TS Two-Stage Test #1: Static Overpressure at 103.8 m.

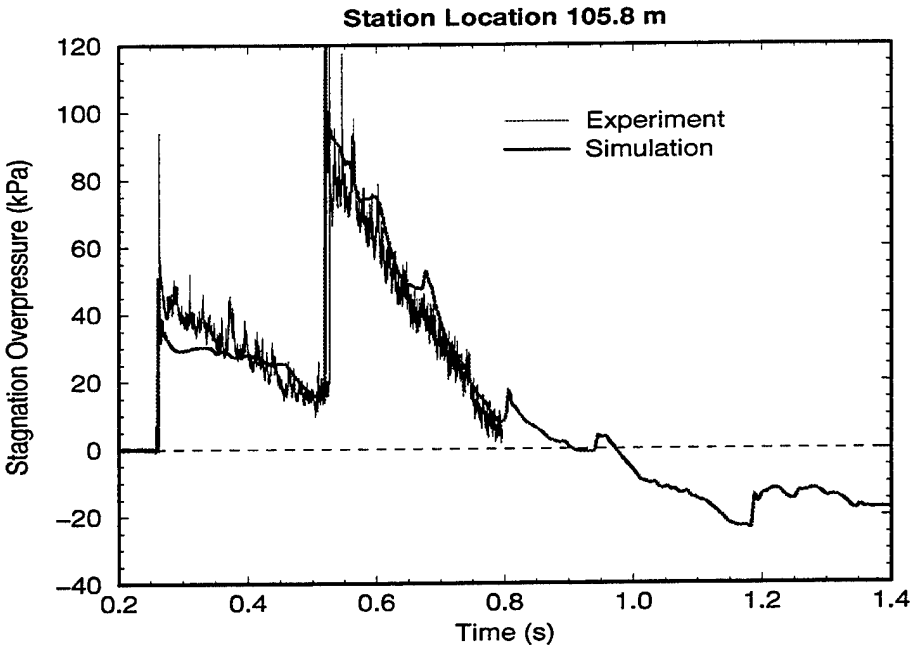

Figure 17. LB/TS Two-Stage Test #1: Stagnation Overpressure at 105.8 m.

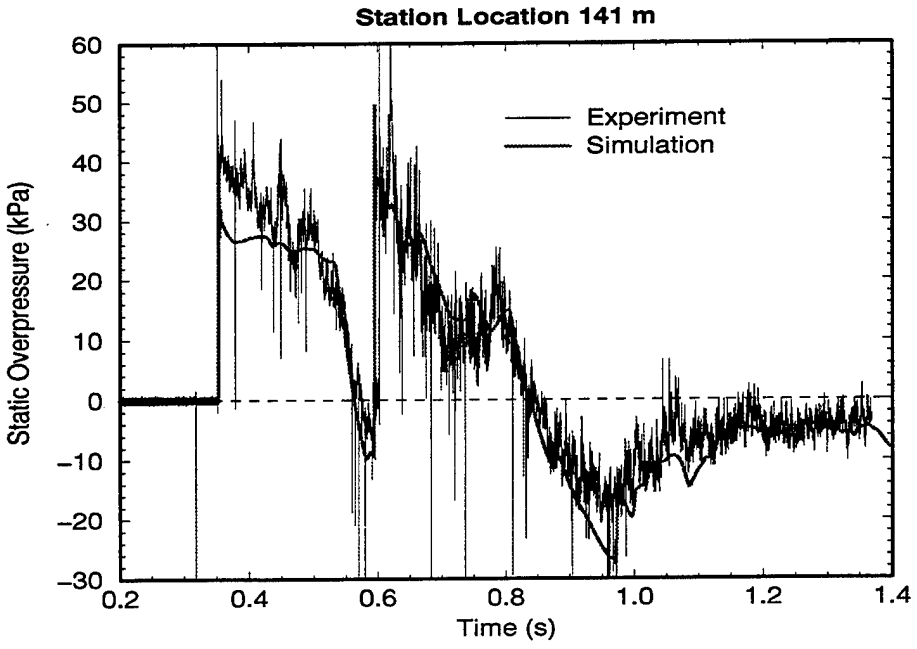

Figure 18. LB/TS Two-Stage Test #1: Static Overpressure at 141 m.

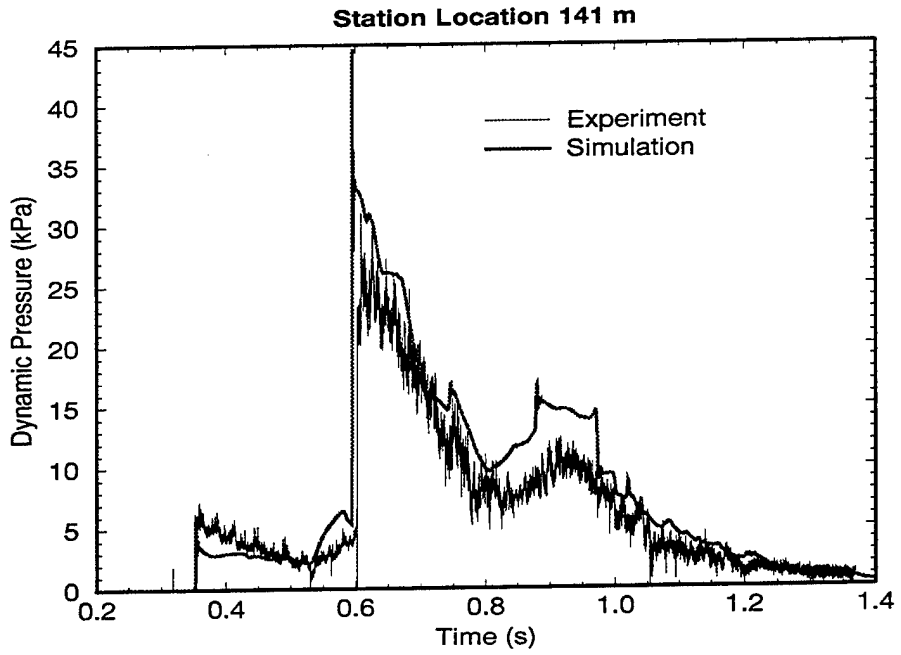

Figure 19. LB/TS Two-Stage Test #1: Dynamic Pressure at 141 m.

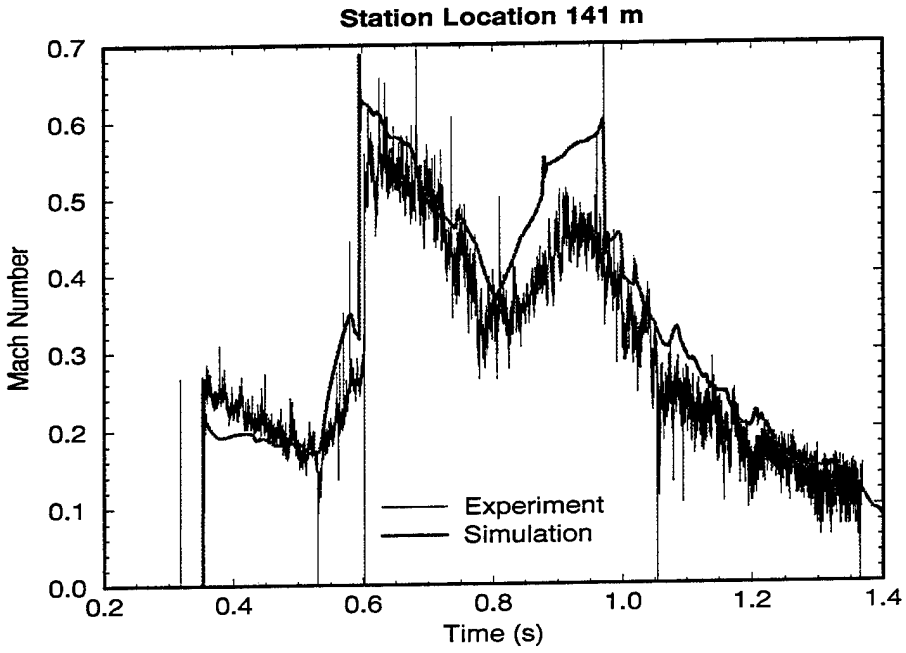

Figure 20. LB/TS Two-Stage Test #1: Mach Number at 141 m.

The stagnation overpressure history recorded at the 141.1-m location and the differential pressure history recorded at 141.2 m were combined to produce the static overpressure, dynamic pressure, and Mach number histories in Figures 18 through 20. These measurements were recorded at a location farther down stream in the tunnel than those provided in Figures 16 and 17 and show that the rarefaction wave arrives at the gauge location shortly before the second shock. The arrival of the rarefaction wave is marked by the sudden decrease in the static overpressure history at 530 ms and the increase in the dynamic pressure and Mach number histories at the same time. The second shock then arrives at 600 ms and combines with the effect of the rarefaction wave to create a second peak in the differential pressure history of approximately 72 kPa. The positive phase of the static overpressure ends at approximately 825 ms for both the experiment and the calculation. In the negative phase of the static overpressure history, a minimum pressure is reached at approximately 975 ms, after which time, the histories asymptotically approach zero.

In the dynamic pressure and Mach number histories in Figures 19 and 20, the computational results closely follow the experimental data after the arrival of the second shock until approximately 800 ms. Between 800 ms and 950 ms, the computed dynamic pressure reaches a value of 15 kPa while the experimental data during this same period is approximately 11 kPa. The Mach number shows a similar over-prediction during this period of time.

The second two-stage test performed in the LB/TS was performed with all the drivers charged to an overpressure of 6.2 MPa and a temperature of 310.9 K. Like the previous test discussed, this test was run with the bank of the five largest drivers fired first, followed 300 ms later by the bank of the four smallest drivers. In this case, all the drivers opened properly. The experiment was performed with a static overpressure gauge at the 103.8-m location, stagnation overpressure gauges at 105.8 m and 155.6 m, and differential pressure gauges at 105.8 m, 141.2 m, and 144.5 m.

The computed and simulated static overpressures for the 103.8-m location are compared in Figure 21. The incident static overpressure produced by the simulation was 28.2% less than that of the experiment. This lower shock amplitude produced by the simulation resulted in a difference in shock arrival time of approximately 8 ms. Despite this late arrival of the incident shock, the simulation properly predicts the arrival time and amplitude of the second shock. From the arrival of the second shock until the end of the positive phase at approximately 825 ms, the computational result closely follows the experimental data.

The experimental histories from the two gauges at the 105.8-m location were used to compute the static overpressure, dynamic pressure, and Mach number histories that are provided in Figures 22, 23, and 24, respectively. Like the history at the 103.8-m location, these figures show the under-prediction of the amplitude of the incident shock, the late arrival of the computed incident shock, and the correct prediction of the arrival time of the second shock. After the arrival of the second shock, the dynamic pressure and Mach number histories pass through the scatter in the experimental data. There is a sudden decrease in the experimental dynamic pressure and Mach number at approximately 1.03 s. This decrease is reproduced in the simulation but occurs approximately 10 ms earlier.

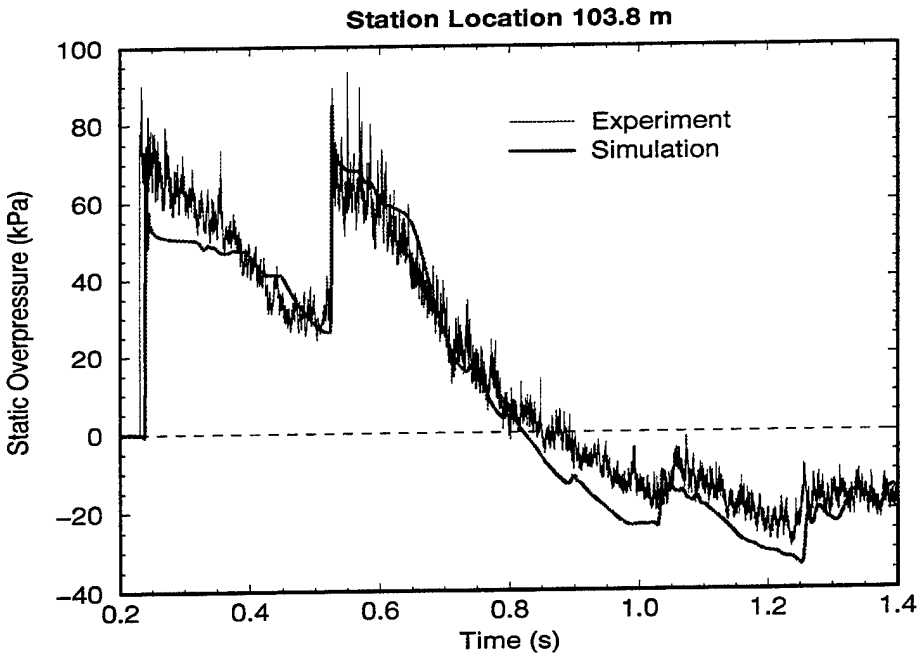

Figure 21. LB/TS Two-Stage Test #2: Static Overpressure at 103.8 m.

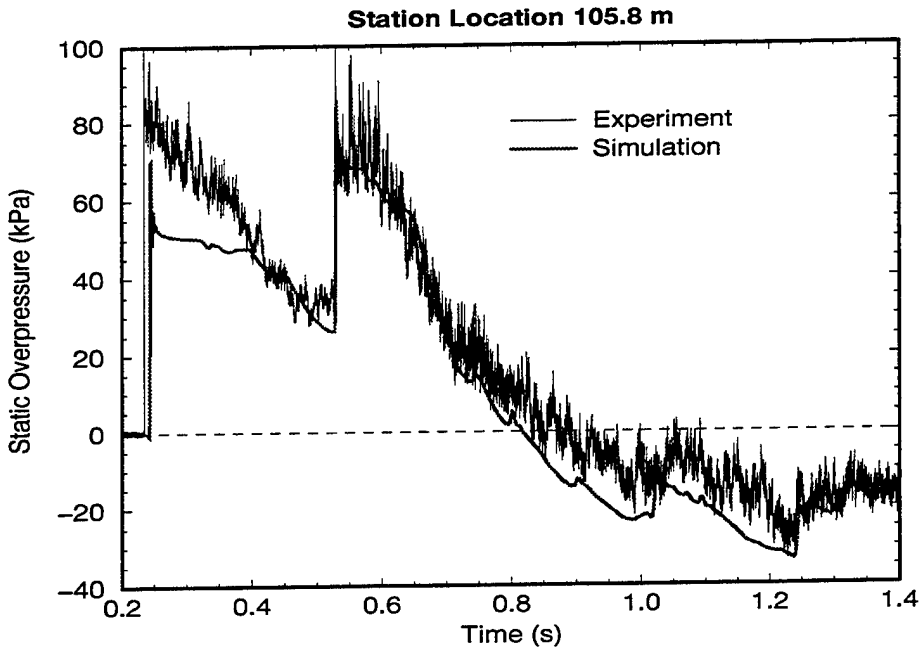

Figure 22. LB/TS Two-Stage Test #2: Static Overpressure at 105.8 m.

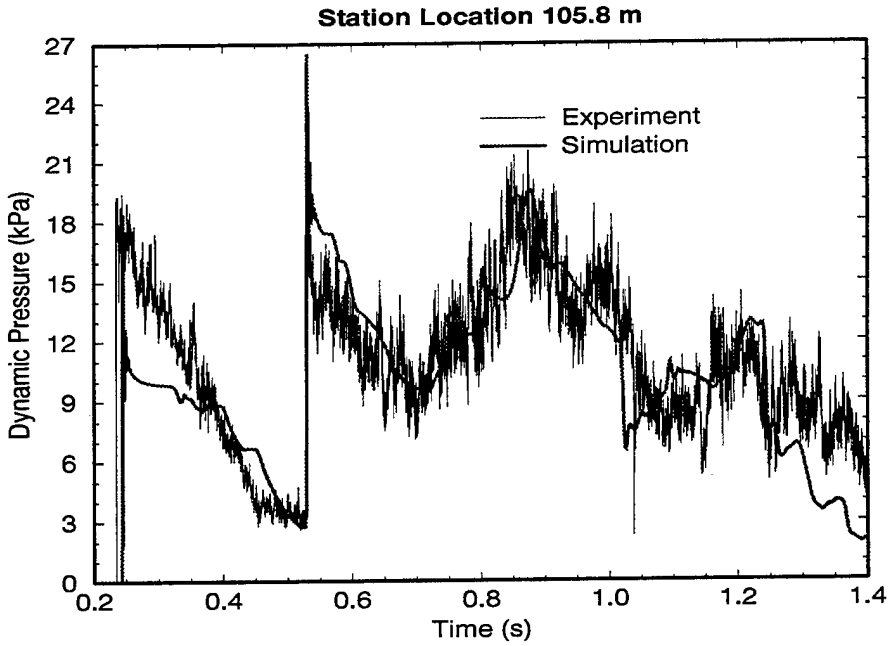

Figure 23. LB/TS Two-Stage Test #2: Dynamic Pressure at 105.8 m.

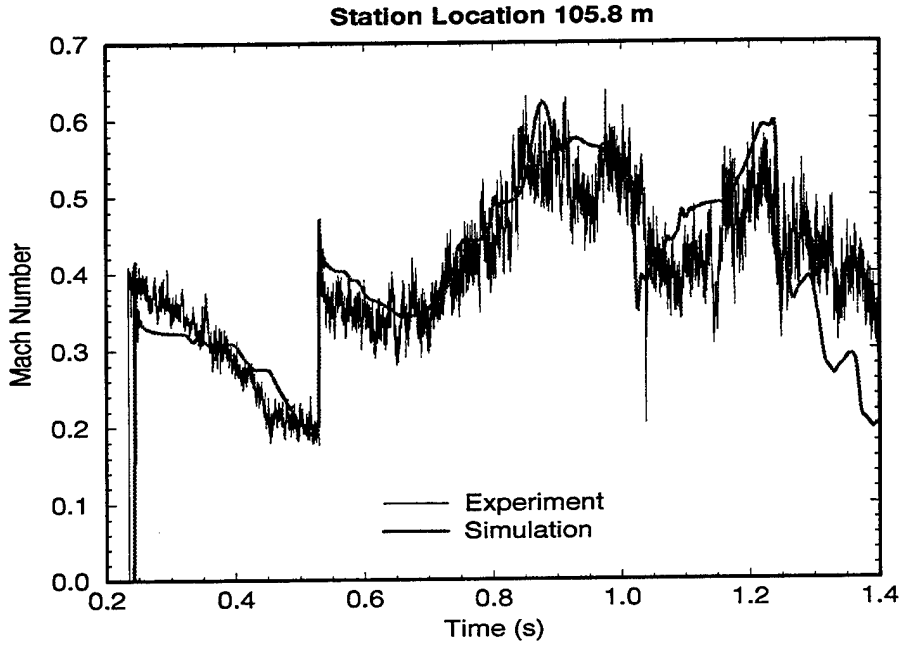

Figure 24. LB/TS Two-Stage Test #2: Mach Number at 105.8 m.

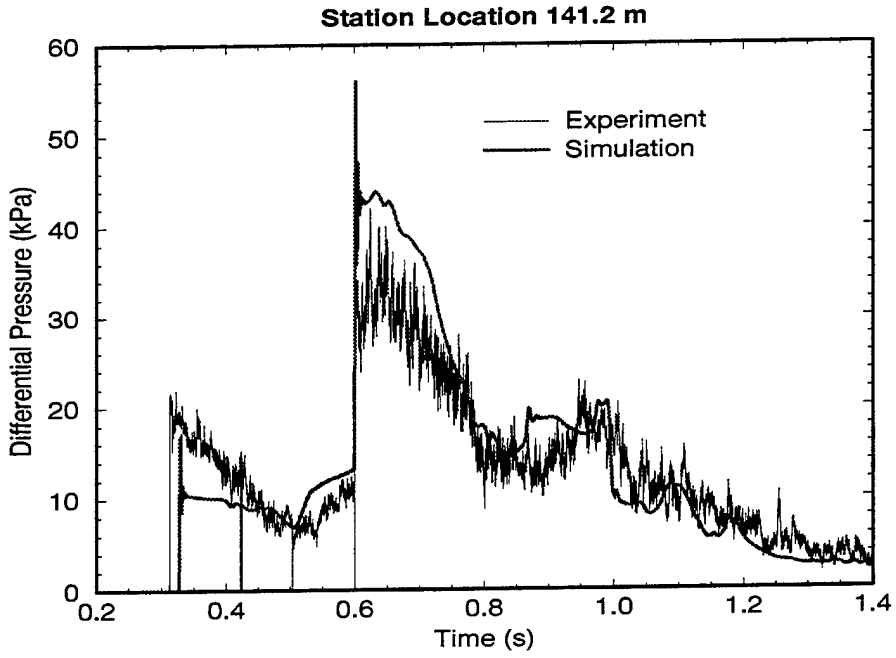

Figure 25. LB/TS Two-Stage Test #2: Differential Pressure at 141.2 m.

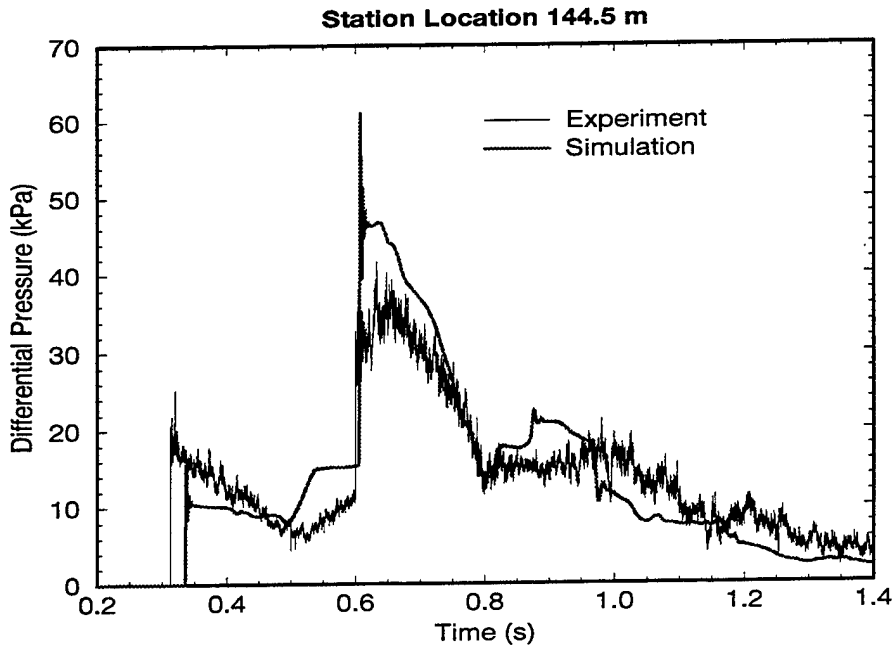

Figure 26. LB/TS Two-Stage Test #2: Differential Pressure at 144.5 m.

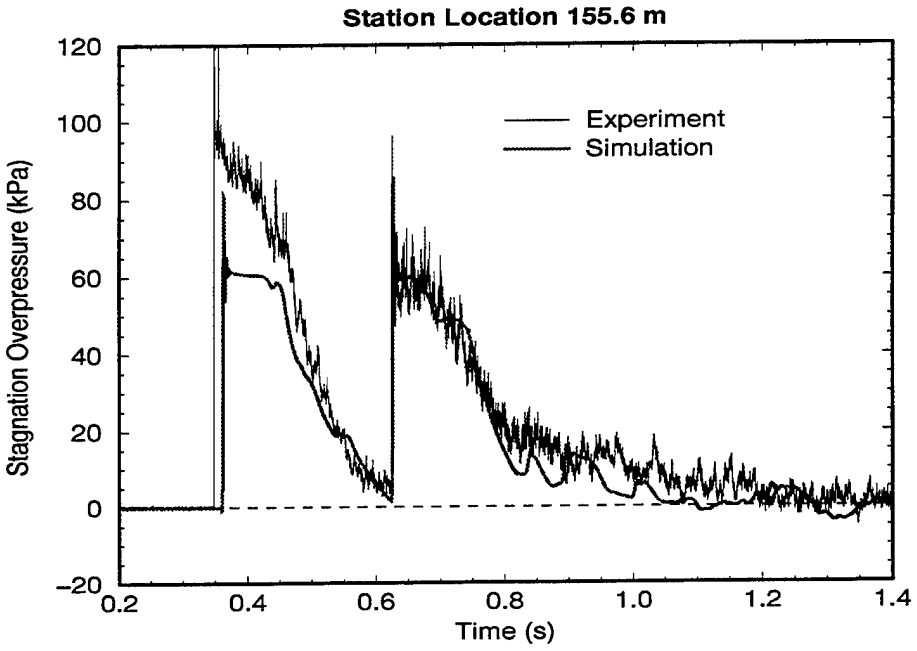

Figure 27. LB/TS Two-Stage Test #2: Stagnation Overpressure at 155.6 m.

Table 5. Summary of Results for LB/TS Two-Stage Test #2.

	Experiment	Simulation	Error
Shock Wave Speed	-	424 m/s	-
Incident Static Overpressure	75.3 kPa	54.1 kPa	-28.2%
Dynamic Pressure Behind Shock	21.2 kPa	11.3 kPa	-46.7%
Mach Number Behind Shock	0.43	0.34	-20.9%
Static Overpressure Impulse at 800 ms (103.8 m)	24.9 kPa-s	23.6 kPa-s	-5.2%
Static Overpressure Impulse at 800 ms (105.8 m)	27.6 kPa-s	23.0 kPa-s	-16.7%
Dynamic Pressure Impulse at 1.4 s (105.8 m)	12.7 kPa-s	12.0 kPa-s	-5.5%
Differential Pressure Impulse at 1.4 s (141.2 m)	14.5 kPa-s	15.2 kPa-s	+4.8%
Differential Pressure Impulse at 1.4 s (144.5 m)	15.3 kPa-s	15.4 kPa-s	+0.7%
Stagnation Overpressure Impulse at 1.4 s (155.6 m)	25.7 kPa-s	19.3 kPa-s	-24.9%

The remaining differential pressure and stagnation overpressure histories are shown in Figures 25 through 27. Because these histories were collected at a location farther down stream, the difference in shock arrival time between the experiment and the calculation is greater than it was at the 105.8-m location, 22 ms to 8 ms. Similar to the first two-stage test, the histories collected close the exit plane of the expansion section show the rarefaction wave arriving at the gauge locations shortly before the second shock. Like the results from the upstream locations, the computation under-predicts the flow conditions behind the incident shock but properly predicts the arrival time of the second shock and the flow histories that follow the second shock.

7.2. Four-Stage Test

The primary purpose of the two-stage staggered driver testing that has been presented here is to produce blast histories with high levels of dynamic pressure. Increasing the initial driver pressure results in increased peak dynamic pressure and dynamic pressure impulse. However, this increase in driver pressure also results in a leading shock of high amplitude. When testing military equipment in such a high dynamic pressure environment, a strong leading shock may cause unwanted structural damage to the target. To decrease the likelihood of causing structural damage with a strong leading shock, it was postulated that the driver gas could be released with a larger number of driver flow stages in the event. This would have the effect of reducing the strength of each individual shock and diffusing the initial shock energy delivery over a set of incremental pressure increases rather than a single, strong shock.

Such a test was performed in the LB/TS. In this test, the primary measurements were made at positions of 103.8 m and 105.8 m from the upstream end of the expansion tunnel. The test consisted of four banks of drivers in which the initial overpressure and temperature were 5.2 MPa and 288.7 K, respectively. Like the two-stage tests, the RWE was not used in order to take advantage of the rarefaction wave that would accelerate the flow in the expansion tunnel and increase the dynamic pressure. The flow field was created by first firing the two 36.2-m driver tubes (t=0 s), then the two 11.0-m tubes at t=100 ms, followed by the three 19.9-m tubes at t=225 ms, and finally the two 28.4-m tubes at t=425 ms. With this configuration, the first two stages of flow were intended to provide shaping of the early time history and introduce dense driver gas into the expansion tunnel. Then, the last two stages were used to further accelerate the gas released by the first two stages.

Just as the two-stage experiment required three calculations to simulate the event, this four-stage test required a total of five calculations to produce the overall simulation. Four independent calculations were performed to simulate the flow from each of the driver banks emptying into the expansion section. The flow histories from these four throat sections were collected and combined using the method described earlier to generate the inlet history in Figure 28.

These histories were then used as a forcing function at the inlet boundary. The cross-sectional area of the inlet boundary of the computational domain was varied with time to

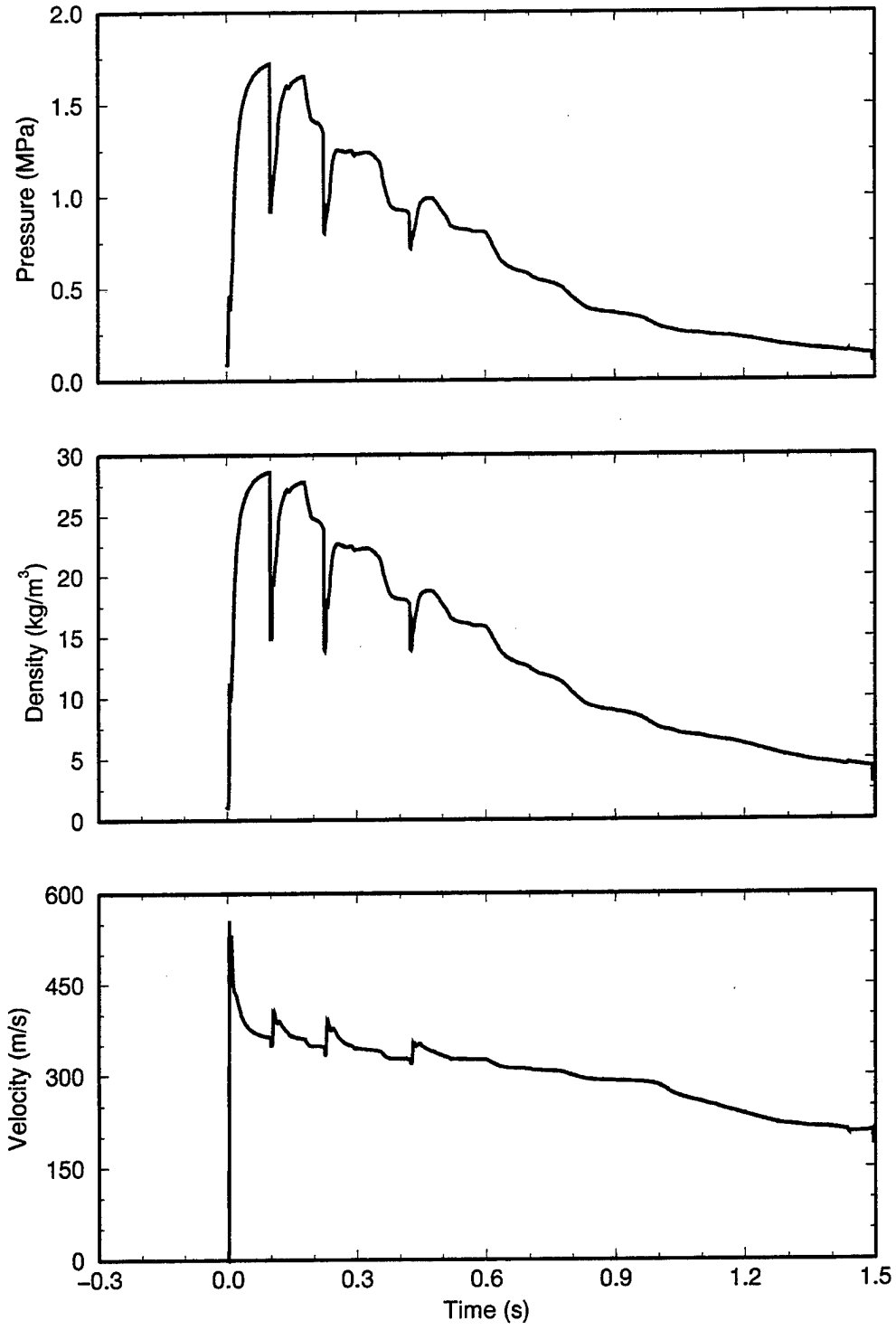

Figure 28. LB/TS Four-Stage Test: Inlet Fluid Histories.

replicate the changes in area associated with the increasing number of drivers during the event. In Figure 29, the inlet boundary area is plotted as a function of time to show the variation in the geometry during the calculation. During the first 100 ms, the inlet cross-sectional area was 1.31 m^2, the sum of the cross-sectional areas of the two throat sections. The area is then increased at the appropriate times to provide the equivalent cross-sectional area of four, seven, and finally nine throat sections. After the last bank of drivers begins to fire, the inlet cross-sectional area is held constant for the remainder of the calculation.

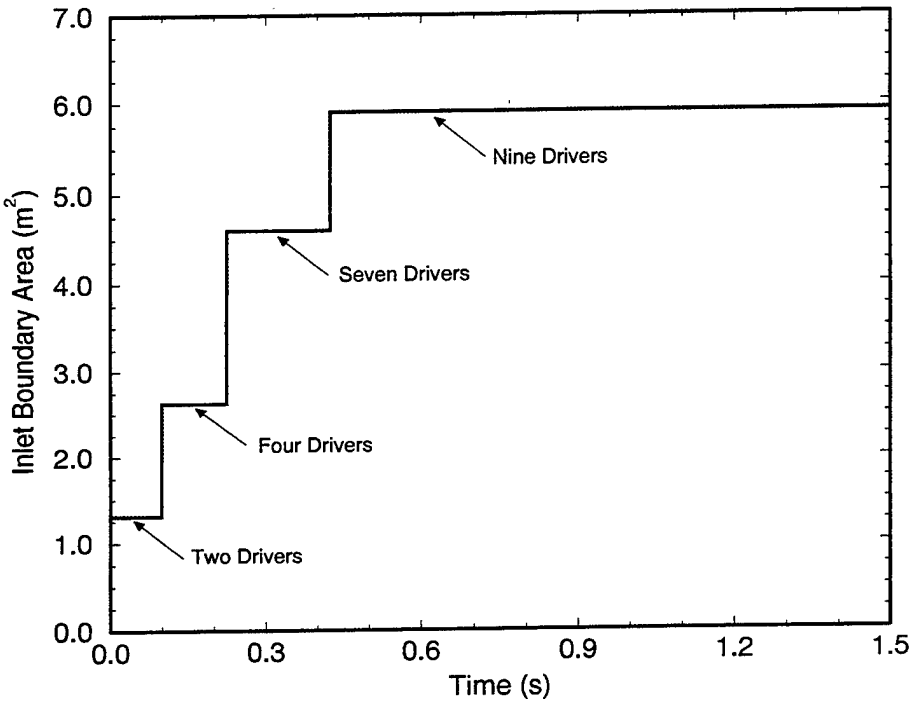

Figure 29. LB/TS Four-Stage Test: Inlet Area History.

A static overpressure gauge was used at the 103.8-m location and its recorded history is compared to the simulation in Figure 30. In this figure, four distinct increases in the experimental and computed histories signify the arrival of the shocks from the individual driver pulses. The computation under-predicts the incident static overpressure by 22% and is the cause of the difference in arrival times of the first shock. The arrival times of the second, third, and fourth shocks in the simulation match those of the experiment. The static overpressure positive phase for the experiment ends at approximately 840 ms, while that of the calculation ends at about 870 ms.

A stagnation overpressure gauge and a differential pressure gauge were employed at the 105.8-m location and were used to generate the static overpressure, dynamic pressure, and Mach number histories of Figures 31, 32, and 33. As in the case of the static overpressure, the computed histories at the 105.8-m location exhibit the dominant flow characteristics

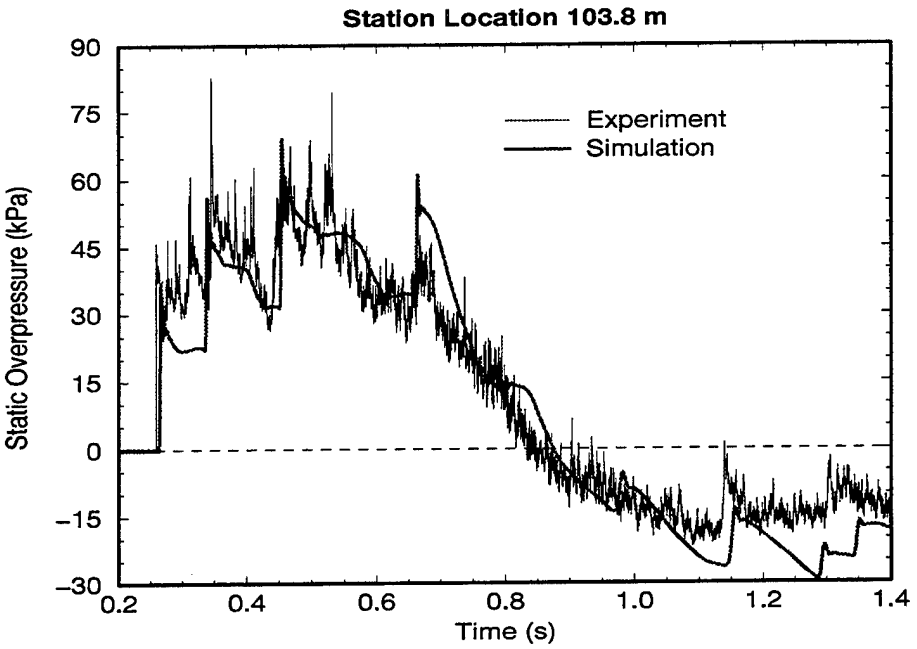

Figure 30. LB/TS Four-Stage Test: Static Overpressure at 103.8 m.

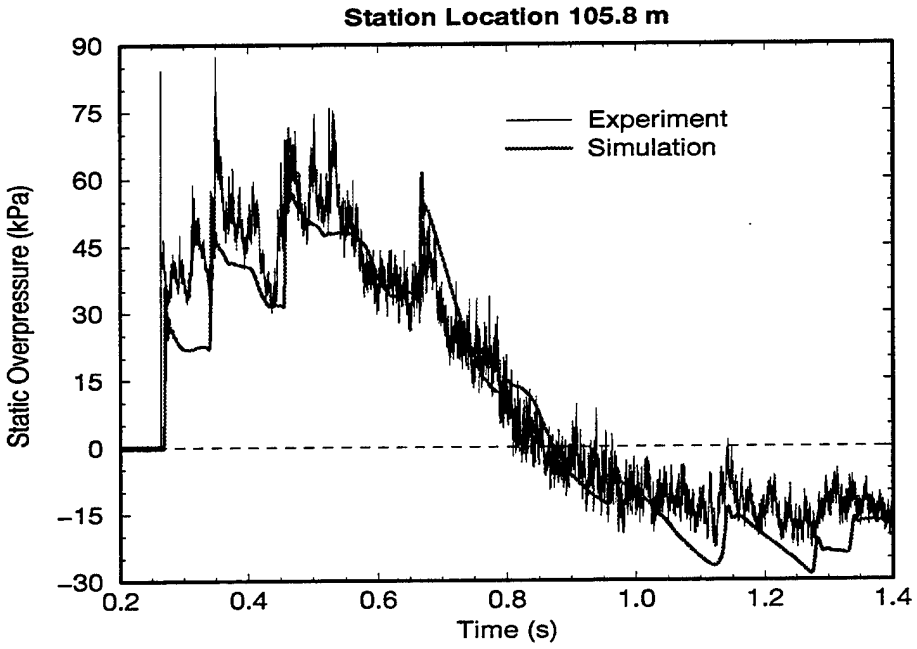

Figure 31. LB/TS Four-Stage Test: Static Overpressure at 105.8 m.

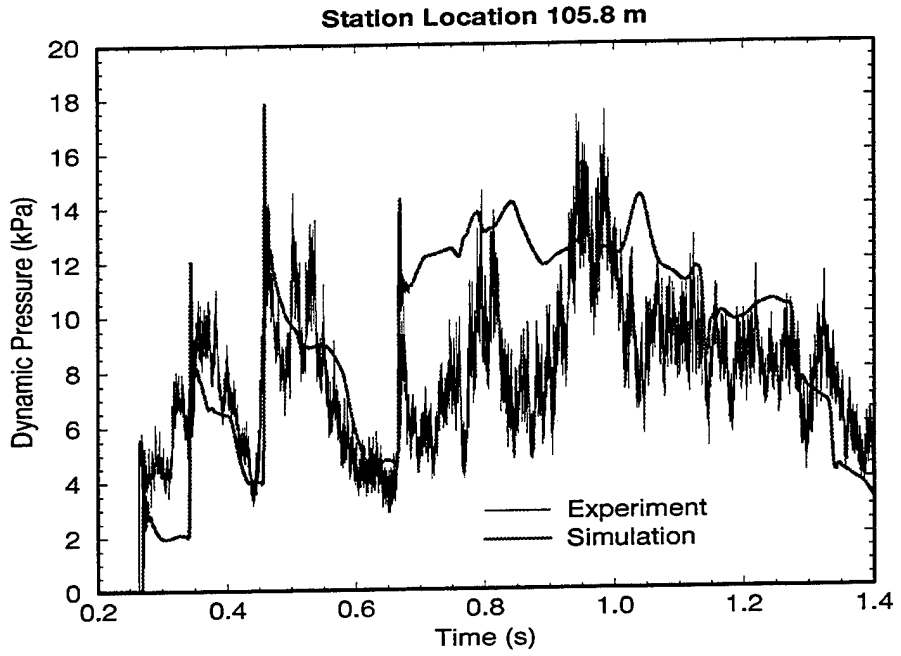

Figure 32. LB/TS Four-Stage Test: Dynamic Pressure at 105.8 m.

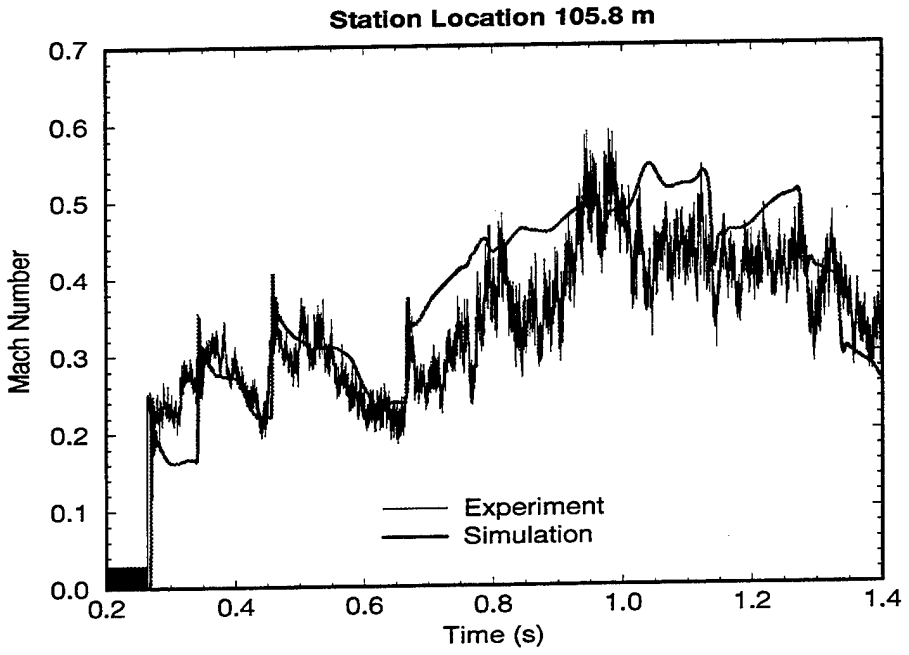

Figure 33. LB/TS Four-Stage Test: Mach Number at 105.8 m.

observed in the experimental data. Table 6 provides additional summary information from the experimental and computational histories.

Table 6. Summary of Results for LB/TS Four-Stage Test.

	Experiment	Simulation	Error
Shock Wave Speed	-	391 m/s	-
Incident Static Overpressure	40.0 kPa	31.2 kPa	-22.0%
Dynamic Pressure Behind Shock	6.3 kPa	3.9 kPa	-38.1%
Mach Number Behind Shock	0.27	0.22	-18.5%
Static Overpressure Impulse at 850 ms (103.8 m)	20.2 kPa-s	20.5 kPa-s	+1.5%
Static Overpressure Impulse at 850 ms (105.8 m)	22.0 kPa-s	20.0 kPa-s	-9.1%
Dynamic Pressure Impulse at 1.4 s (105.8 m)	8.9 kPa-s	10.4 kPa-s	+16.9%

8. SUMMARY

This report has documented the development and validation of a computational tool for simulating complex flow fields in shock tubes and blast simulators. The tool is easy to use and requires only 20 to 30 lines of input data to completely define a geometry, boundary conditions, initial fluid conditions, and run control information. Most of the calculations illustrated in this report required only a few minutes of run time to complete on an average workstation. The most complex staggered flow calculation ran in about 1 hour. With its ease of use and quick turn-around time, this code makes it possible to perform complex flow studies consisting of numerous calculations in a short period of time. These traits make the code well suited as a design tool for shock tube experiments or for deriving first order estimates of flow fields for large 3-D computational studies.

The variety of shock tube geometries presented here provides an indication of the capabilities and limitations of the code. Overall, the code performed best in simulating shock tubes with simple geometries. Differences between computed and experimental flow histories were greatest when simulating the most complex geometries. For the single stage flow cases, the predictions of the incident static overpressure were typically within 10% of the experimental results. For these same cases, the difference between the simulated and experimental static and dynamic impulses was less than 20%.

For multi-staged shock tube flows, the code inherently under-prediced the amplitude of the leading shock but generally followed the dominant trends in the experimental flow histories. The error in the prediction of the incident static overpressure was greatest for the second two-stage test and was 28.2%. The difference in impulse values between the experiment and computation was typically less than 15% for the multi-staged flows. The code demonstrated that it can accurately reproduce the arrival times of multiple shocks in a multi-stage event, making it a useful tool for designing experiments that require such flow characteristics.

INTENTIONALLY LEFT BLANK

REFERENCES

1. Glasstone, S. and P. Dolan - Editors. "The Effects of Nuclear Weapons." Department of Army Pamphlet No. 50-3, HQ, Department of Army. March 1977.

2. Hikida, S., R. Bell, and C. Needham. "The SHARC Codes: Documentation and Sample Problems." S-Cubed Technical Report SSS-R-89-9878. September 1988.

3. Chakravarthy, S., K. Szema, U. Goldberg, J. Gorski and S. Osher. "Application of a New Class of High Accuracy TVD Schemes to the Navier-Stokes Equations." AIAA Paper 85-0165. January 1985.

4. Schraml, S.J. and C. Mermagen. "Experimental Evaluation and Numerical Simulations of Multi-Driver Shock Tube Flow." U.S. Army Research Laboratory Technical Report ARL-TR-1084. Aberdeen Proving Ground, MD. April 1996.

5. Schraml, S.J."Performance Predictions for the Large Blast/Thermal Simulator Based on Experimental and Computational Results." U.S. Army Ballistic Research Laboratory Technical Report BRL-TR-3232. Aberdeen Proving Ground, MD. May 1991.

6. Kundu, P.K. *Fluid Mechanics.* Academic Press, Inc. ISBN 0-12-428770-0 1990.

7. Fletcher, C.A.J. *Computational Techniques for Fluid Dynamics - Volume II.* Springer-Verlag. ISBN 0-387-53601-9 1991.

8. MacCormack, R.W. "The Effect of Viscosity in Hypervelocity Impact Cratering." AIAA Paper 69-354. 1969.

9. Roache, P.J. *Computational Fluid Dynamics.* Hermosa Publishers. Albuquerque, NM. 1972

10. Zucrow, M.J. and J.D. Hoffman. *Gas Dynamics.* John Wiley & Sons. New York, NY. ISBN 0-471-98440-X. 1976.

11. Ethridge, N.E. "Proposed Design for a Differential Pressure Gage to Measure Dynamic Pressure in Blast Waves." U.S. Army Ballistic Research Laboratory Memorandum Report BRL-MR-2814. Aberdeen Proving Ground, MD. August 1978.

12. Coulter, G.A. and B.P. Bertrand. "BRL Shock Tube Facility for the Simulation of Air Blast Effects." U.S. Army Ballistic Research Laboratory Memorandum Report BRL-MR-1685. Aberdeen Proving Ground, MD. August 1965.

13. Fletcher, C.A.J. *Computational Techniques for Fluid Dynamics - Volume I.* Springer-Verlag. ISBN 3-540-53601-9 1991.

14. Engineering Design Handbook *Explosions in Air - Part One.* U.S. Army Materiel Command Pamphlet AMCP-706-181. Alexandria, VA. July 1974.

15. Mihalcin, A.L. "Performance Predictions for the ARL Enhanced 2.44-m Blast Simulator." U.S. Army Research Laboratory Technical Report ARL-TR-1162. Aberdeen Proving Ground, MD. June 1996.

16. Schraml, S.J. and R.J. Pearson. "Small Scale Shock Tube Experiments Using a Computer Controlled Active Rarefaction Wave Eliminator." U.S. Army Ballistic Research Laboratory Technical Report BRL-TR-3149. September 1990.

17. Ethridge, N.H. et al. "Real Surface (Non-Ideal) Effects on Nuclear Explosion Airblast from PRISCILLA-Type Events." U.S. Army Research Laboratory Contract Report ARL-CR-277. October 1995.

NO. OF COPIES	ORGANIZATION
2	ADMINISTRATOR DEFENSE TECHNICAL INFO CENTER ATTN DTIC DDA 8725 JOHN J KINGMAN RD STE 0944 FT BELVOIR VA 22060-6218
1	DIRECTOR US ARMY RESEARCH LABORATORY ATTN AMSRL OP SD TA/ RECORDS MANAGEMENT 2800 POWDER MILL RD ADELPHI MD 20783-1197
1	DIRECTOR US ARMY RESEARCH LABORATORY ATTN AMSRL OP SD TL/ TECHNICAL LIBRARY 2800 POWDER MILL RD ADELPHI MD 207830-1197
1	DIRECTOR US ARMY RESEARCH LABORATORY ATTN AMSRL OP SD TP/ TECH PUBLISHING BRANCH 2800 POWDER MILL RD ADELPHI MD 20783-1197
2	HQDA (SARD TR/MS K KOMINOS) (SARD TR/DR R CHAIT) WASHINGTON DC 20310-0103
2	DIRECTOR FEDERAL EMERGENCY MGMT AGENCY ATTN PUBLIC RELATIONS OFFICE TECHNICAL LIBRARY WASHINGTON DC 20472
2	HQDA (SARD TT/MS C NASH) (SARD TT/DR F MILTON) WASHINGTON DC 20310-0103
1	CHAIRMAN DOD EXPLOSIVES SAFETY BOARD ROOM 856 C HOFFMAN BLDG 1 2461 EISENHOWER AVENUE ALEXANDRIA VA 22331-0600
1	DIRECTOR OF DEFENSE RESEARCH AND ENGINEERING ATTN DD/TWP WASHINGTON DC 20301

NO. OF COPIES	ORGANIZATION
1	DIRECTOR DEFENSE INTELLIGENCY AGENCY ATTN DT 2/WPNS & SYS DIVISION WASHINGTON DC 20301
1	ASST SECRETARY OF DEFENSE (ATOMIC ENERGY ATTN DOCUMENT CONTROL WASHINGTON DC 20301
6	DIRECTOR DEFENSE NUCLEAR AGENCY ATTN CSTI TECHNICAL LIBRARY ESA W SUMMA E SEIDEN K PETERSEN WEP T KENNEDY M FRANKEL WASHINGTON DC 20305
1	CHAIRMAN JOINT CHIEFS OF STAFF ATTN J 5 R&D DIVISION WASHINGTON DC 20301
2	DA DCSOPS ATTN TECHNICAL LIBRARY DIR OF CHEM & NUC OPS WASHINGTON DC 20310
4	COMMANDER FIELD COMMAND DNA ATTN FCTTS E MARTINEZ FCTOSL F MOYNIHAN FCTIH H ROSS FCTIH W BRENNAN KIRTLAND AFB NM 87115
10	CENTRAL INTELLIGENCE AGENCY DIR/DB/STANDARD ATTN GE 47 HQ WASHINGTON DC 20505
1	DIRECTOR ADVANCED RSCH PROJECTS AGENCY ATTN TECHNICAL LIBRARY 3701 NORTH FAIRFAX DRIVE ARLINGTON VA 22203-1714
2	COMMANDER US ARMY CECOM ATTN AMSEL RD AMSEL RO TPPO P FORT MONMOUTH NJ 07703-5301

NO. OF COPIES	ORGANIZATION
1	COMMANDER US ARMY CECOM R&D TECHNICAL LIBRARY ATTN ASQNC ELC IS L R MYER CTR FORT MONMOUTH NJ 07703-5000
1	MIT ATTN TECHNICAL LIBRARY CAMBRIDGE MA 02139
1	COMMANDER US ARMY FSTC ATTN RESEARCH & DATA BRANCH 220 7TH STREET NE CHARLOTTESVILLE VA 22901-5396
1	COMMANDER US ARMY ARDEC ATTN SMCAR FSM W/BARBER BLDG94 PICATINNY ARSENAL NJ 07806-5000
1	DIRECTOR US ARMY MISSILE & SPACE INTELLIGENCE CENTER ATTN AIAMS YDL REDSTONE ARSENAL AL 35898-5500
1	COMMANDING OFFICER (CODE L51) NAVAL CIVIL ENGINEERING LAB ATTN J TANCRETO PORT HUENEME CA 93043-5003
2	COMMANDER US ARMY STRATEGIC DEFENSE CMD ATTN CSSD H MPL TECH LIB CSSD H XM DR DAVIES PO BOX 1500 HUNTSVILLE AL 35807
2	COMMANDER US ARMY CORPS OF ENGINEERS WATERWAYS EXPERIMENT STA ATTN CEWES SS R J WATT CEWES TL TECH LIBRARY PO BOX 631 VICKSBURG MS 39180-0631
1	COMMANDER US ARMY ENGINEER DIVISION ATTN HNDED FD PO BOX 1500 HUNTSVILLE AL 35807

NO. OF COPIES	ORGANIZATION
3	COMMANDER US ARMY NUCLEAR & CHEM AGENCY 7150 HELLER LOOP SUITE 101 SPRINGFIELD VA 22150-3198
1	COMMANDER US ARMY CORPS OF ENGINEERS FT WORTH DISTRICT ATTN CESWF PM J PO BOX 17300 FORT WORTH TEXAS 76102-0300
1	DIRECTOR TRAC FLVN ATTN ATRC FORT LEAVENWORTH KS 66027-5200
1	COMMANDER US ARMY RESEARCH OFFICE ATTN SLCRO D PO BOX 12211 RESEARCH TRIANGLE PARK NC 27709-2211
1	DIRECTOR HQ TRAC RPD ATTN ATRC RPR RADDA FORT MONROE VA 23651-5143
2	OFFICE OF NAVAL RESEARCH ATTN DR A FAULSTICK CODE 23 800 N QUINCY STREET ARLINGTON VA 22217
1	DIRECTOR TRAC WSMR ATTN ATRC WC KIRBY WSMR NM 88002-5502
2	COMMANDER US ARMY WSMR ATTN STEWS NED (DR MEASON) STEWS DATTS O (RL PENNY) WSMR NM 88002-5158
2	CHIEF OF NAVAL OPERATIONS DEPARTMENT OF THE NAVY ATTN OP 03EG OP 985F WASHINGTON DC 20350
1	COMMANDER DAVID TAYLOR RESEARCH CENTER ATTN CODE 522 TECH INFO CTR BETHESDA MD 20084-5000

NO. OF COPIES	ORGANIZATION
1	OFFICER IN CHARGE (CODE L31) CIVIL ENGINEERING LABORATORY NAVAL CONST BATTALION CENTER ATTN TECHNICAL LIBRARY PORT HUENEME CA 93041
1	COMMANDER (CODE 533) NAVAL WEAPONS CENTER ATTN TECHNICAL LIBRARY CHINA LAKE CA 93555-6001
1	COMMANDER DAHLGREN DIVISION NAVAL SURFACE WARFARE CENTER ATTN CODE E23 LIBRARY DAHLGREN VA 22448-5000
1	COMMANDER NAVAL RESEARCH LABORATORY ATTN CODE 2027 TECH LIBRARY WASHINGTON DC 20375
1	OFFICER IN CHARGE WHITE OAK WARFARE CENTER DETACHMENT ATTN CODE E232 TECH LIBRARY 10901 NEW HAMPSHIRE AVENUE SILVER SPRING MD 20903-5000
1	AL/LSCF ATTN J LEVINE EDWARDS AFB CA 93523-5000
1	COMMANDER NAVAL WEAPONS EVALUATION FAC ATTN DOCUMENT CONTROL KIRTLAND AFB NM 87117
1	RADC (EMTLD/DOCUMENT LIB) GRIFFISS AFB NY 13441
1	AEDC ATTN R MCAMIS MAIL STOP 980 ARNOLD AFB TN 37389
1	OLAC PL/TSTL ATTN D SHIPLETT EDWARDS AFB CA 93523 5000
1	AFIT/ENY ATTN LTC HASEN PHD WRIGHT PATTERSON AFB OH 45433-6583

NO. OF COPIES	ORGANIZATION
2	AIR FORCE ARMAMENT LAB ATTN AFATL/DOIL AFATL/DLYV EGLIN AFB FL 32542-5000
1	DIRECTOR IDAHO NATIONAL ENGINEERING LAB ATTN SPEC PROGRAMS J PATTON 2151 NORTH BLVD MS 2802 IDAHO FALLS ID 83415
3	PHILLIPS LABORATORY (AFWL) ATTN NTE NTED NTES KIRTLAND AFB NM 87117-6008
1	DIRECTOR LAWRENCE LIVERMORE NATL LAB ATTN TECH INFO DEPT L 3 PO BOX 808 LIVERMORE CA 94550
1	AFIT ATTN TECHNICAL LIBRARY BLDG 640/B WRIGHT PATTERSON AFB OH 45433
1	DIRECTOR NATL AERONAUTICS & SPACE ADMIN ATTN SCIENTIFIC & TECH INFO FAC PO BOX 8757 BWI AIRPORT BALTIMORE MD 21240
1	FTD/NIIS WRIGHT PATTERSON AFB OH 45433
3	KAMAN SCIENCES CORPORATION ATTN LIBRARY PA ELLIS FH SHELTON PO BOX 7463 COLORADO SPRINGS CO 80933-7463
4	DIRECTOR IDAHO NATIONAL ENGINEERING LAB EG&G IDAHO INC ATTN R GUENZLER MS 3505 R HOLMAN MS 3510 R A BERRY W C REED PO BOX 1625 IDAHO FALLS ID 83415

NO. OF COPIES	ORGANIZATION
4	DIRECTOR SANDIA NATIONAL LABORATORIES ATTN DOC CONTROL 3141 D GARDNER DIV 1421 J MCGLAUN DIV 1541 PO BOX 58O0 ALBUQUERQUE NM 87185-5800
2	LOS ALAMOS NATL LABORATORY MAIL STATION 5000 REPORT COLLECTION CID 14 MS P364 PO BOX 1663 LOS ALAMOS NM 87545
1	REPORT COLLECTION CIC 14 MS P364 LOS ALAMOS NATL LABORATORY LOS ALAMOS NM 87545
1	REPORT COLLECTION RESEARCH LIBRARY MS P362 PO BOX 7113 LOS ALAMOS NM 87544-7113
1	DIRECTOR SANDIA NATIONAL LABORATORIES LIVERMORE LABORATORY ATTN DOC CONTROL FOR TECH LIB PO BOX 969 LIVERMORE CA 94550
1	DIRECTOR NASA LANGLEY RESEARCH CENTER ATTN TECHNICAL LIBRARY HAMPTON VA 23665
2	APPLIED RESEARCH ASSOCIATES INC ATTN J KEEFER NH ETHRIDGE PO BOX 548 ABERDEEN MD 21001
4	APPLIED RESEARCH ASSOCIATES INC ATTN C NEEDHAM J CREPEAU S HIKIDA R NEWELL 4300 SAN MATEO BLVD ALBUQUERQUE NM 87110
1	ADA TECHNOLOGIES INC ATTN JAMES R BUTZ HONEYWELL CENTER SUITE 110 304 INVERNESS WAY SOUTH ENGLEWOOD CO 80112

NO. OF COPIES	ORGANIZATION
1	CARPENTER RESEARCH CORP ATTN H JERRY CARPENTER 27520 HAWTHORNE BLVD SUITE 263 PO BOX 2490 ROLLING HILLS ESTATES CA 90274
1	AEROSPACE CORPORATION ATTN TECH INFO SERVICES PO BOX 92957 LOS ANGELES CA 90009
1	THE BOEING COMPANY ATTN AEROSPACE LIBRARY PO BOX 3707 SEATTLE WA 98124
2	FMC CORPORATION ADVANCED SYSTEMS CENTER ATTN J DROTLEFF C KREBS MDP 95 BOX 58123 2890 DE LA CRUZ BLVD SANTA CLARA CA 95052
1	SVERDRUP TECHNOLOGY INC SVERDRUP CORPORATION AEDC ATTN BD HEIKKINEN MS 900 ARNOLD AFB TN 37389-9998
1	DYNAMICS TECHNOLOGY INC ATTN D T HOVE G P MASON 21311 HAWTHORNE BLVD SUITE 300 TORRANCE CA 90503
1	KTECH CORPORATION ATTN DR E GAFFNEY 901 PENNSYLVANIA AVE NE ALBUQUERQUE NM 87111
1	EATON CORPORATION DEFENSE VALVE & ACTUATOR DIV ATTN J WADA 2338 ALASKA AVE EL SEGUNDO CA 90245-4896
2	MCDONNELL DOUGLAS ASTRO- NAUTICS CORP ATTN R W HALPRIN K A HEINLY 5301 BOLSA AVENUE HUNTINGTON BEACH CA 92647

NO. OF COPIES	ORGANIZATION
4	KAMAN AVIDYNE ATTN R RUETENIK S CRISCIONE R MILLIGAN T STAGLIANO 83 SECOND AVENUE NORTHWEST INDUSTRIAL PARK BURLINGTON MA 01830
1	MDA ENGINEERING INC ATTN DR DALE ANDERSON 500 EAST BORDER STREET SUITE 401 ARLINGTON TX 07601
2	POINTWISE INC ATTN J CHAWNER J STEINBRENNER PO BOX 210698 BEDFORD TX 76095-7698
2	PHYSICS INTERNATIONAL CORP PO BOX 5010 SAN LEANDRO CA 94577-0599
2	KAMAN SCIENCES CORPORATION ATTN DASIAC (2CYS) PO DRAWER 1479 816 STATE STREET SANTA BARBARA CA 93102-1479
1	LOGICON RDA ATTN GP GANONG PO BOX 9377 ALBUQUERQUE NM 87119
1	LOGICON RDA ATTN B LEE 6053 W CENTURY BLVD LOS ANGELES CA 90045
1	LOCKHEED MISSILES & SPACE CO ATTN J J MURPHY DEPT 81 11 BLDG 154 PO BOX 504 SUNNYVALE CA 94086
1	SCIENCE CENTER ROCKWELL INTERNATIONAL CORP ATTN S RAMAKRISHNAN D OTA 1049 CAMINO DOS RIOS PO BOX 2085 THOUSAND OAKS CA 91358

NO. OF COPIES	ORGANIZATION
1	METACOMP TECHNOLOGIES INC ATTN S CHAKRAVARTHY 650 WESTLAKE BLVD SUITE 203 WESTLAKE VILLAGE CA 91362
1	ORLANDO TECHNOLOGY INC ATTN D MATUSKA 60 SECOND STREET BLDG 5 SHALIMAR FL 32579
4	S CUBED A DIVISION OF MAXWELL LABS INC ATTN TECHNICAL LIBRARY R DUFF K PYATT J BARTHEL PO BOX 1620 LA JOLLA CA 92037-1620
1	SAICORPORATION ATTN J GUEST 2301 YALE BLVD SE SUITE E ALBUQUERQUE NM 87106
1	SUNBURST RECOVERY INC ATTN DR C YOUNG PO BOX 2129 STEAMBOAT SPRINGS CO 80477
1	SVERDRUP TECHNOLOGY INC ATTN RF STARR PO BOX 884 TULLAHOMA TN 37388
1	S CUBED A DIVISION OF MAXWELL LABS INC ATTN JAMES SEVIER 2501 YALE BLVD SE ALBUQUERQUE NM 87106
3	SRI INTERNATIONAL ATTN DR GR ABRAHAMSON DR J GRAN DR B HOLMES 333 RAVENWOOD AVENUE MENLO PARK CA 94025
1	TRW BALLISTIC MISSILE DIVISION ATTN H KORMAN MAIL STATION 526/614 PO BOX 1310 SAN BERNADINO CA 92402

NO. OF COPIES	ORGANIZATION
1	BATTELLE ATTN TACTEC LIB JN KHIGGINS 505 KING AVENUE COLUMBUS OH 43201-2693
1	THERMAL SCIENCE INC ATTN R FELDMAN 2200 CASSENS DRIVE ST LOUIS MO 63026
2	DENVER RESEARCH INSTITUTE ATTN J WISOTSKI TECHNICAL LIBRARY PO BOX 10758 DENVER CO 80210
1	STATE UNIVERSITY OF NEW YORK MECH & AEROSPACE ENGINEERING ATTN DR PEYMAN GIVI BUFFALO NY 14260
2	UNIVERSITY OF MARYLAND INST FOR ADV COMPUTER STUDIES ATTN L DAVIS G SOBIESKI COLLEGE PARK MD 20742
1	CALIFORNIA INST OF TECHNOLOGY ATTN T J AHRENS 1201 E CALIFORNIA BLVD PASADENA CA 91109
1	UNIVERSITY OF MINNESOTA ARMY HIGH PERF COMP RES CTR ATTN DR TAYFUN E TEZDUYAR 1100 WASHINGTON AVE SOUTH MINNEAPOLIS MN 55415
3	SOUTHWEST RESEARCH INSTITUTE ATTN DR C ANDERSON S MULLIN A B WENZEL PO DRAWER 28255 SAN ANTONIO TX 78228-0255
2	COMMANDER US ARMY NRDEC ATTN SSCNC YSD (J ROACH) SSCNC WST (A MURPHY) KANSAS STREET NATICK MA 10760-5018

NO. OF COPIES	ORGANIZATION
	ABERDEEN PROVING GROUND
2	DIR ARL ATTN AMSRL OP AP L (TECH LIB) BLDG 305 APG
1	COMMANDER US ARMY TECOM ATTN AMSTE TE F (L TELETSKI) RYAN BLDG APG
1	COMMANDER US ARMY THAMA ATTN AMSTH TE APG -EA
1	COMMANDER US ARMY TEST CENTER ATTN STEC LI APG
15	DIRECTOR US ARMY RESEARCH LABORATORY ATTN AMSRL CI H C NIETUBICZ AMSRL CI HC J COLLINS J GROSH D HISLEY AMSRL IS B A MARK R PEARSON AMSRL SL CM E FIORVANTE AMSRL WM PB P PLOSTINS P WEINACHT B GUIDOS AMSRL WM TB R FREY R LOTTERO J STARKENBERG AMSRL WM TC W DEROSSET K KIMSEY

REPORT DOCUMENTATION PAGE

Form Approved
OMB No. 0704-0188

1. AGENCY USE ONLY *(Leave blank)*	2. REPORT DATE	3. REPORT TYPE AND DATES COVERED
	November 1996	Final

4. TITLE AND SUBTITLE

A One-Dimensional Numerical Method for Simulating Multiple Stage Shock Tube Flows

5. FUNDING NUMBERS

PR: 68N522

6. AUTHOR(S)

Schraml, S.J.

7. PERFORMING ORGANIZATION NAME(S) AND ADDRESS(ES)

U.S. Army Research Laboratory
Weapons & Materials Research Directorate
Aberdeen Proving Ground, MD 21010-5066

8. PERFORMING ORGANIZATION REPORT NUMBER

9. SPONSORING/MONITORING AGENCY NAME(S) AND ADDRESS(ES)

U.S. Army Research Laboratory
Weapons & Materials Research Directorate
Aberdeen Proving Ground, MD 21010-5066

10. SPONSORING/MONITORING AGENCY REPORT NUMBER

ARL-TR-1255

11. SUPPLEMENTARY NOTES

12a. DISTRIBUTION/AVAILABILITY STATEMENT

Approved for public release; distribution is unlimited.

12b. DISTRIBUTION CODE

13. ABSTRACT *(Maximum 200 words)*

A method is presented for the numerical simulation of time-dependent fluid flow in shock tubes and blast simulators. This method solves the Euler equations in a one-dimensional (1-D) computational domain with area changes. Complex flow fields can be simulated through the use of grid geometries and boundary conditions that are allowed to vary with time. The formulation of the solution algorithm and the time-varying boundary conditions are described. Results of a set of benchmark calculations are presented to illustrate the capabilities of the technique.

14. SUBJECT TERMS

blast
fluid dynamics
flow fields
shock tubes

15. NUMBER OF PAGES

50

16. PRICE CODE

17. SECURITY CLASSIFICATION OF REPORT	18. SECURITY CLASSIFICATION OF THIS PAGE	19. SECURITY CLASSIFICATION OF ABSTRACT	20. LIMITATION OF ABSTRACT
Unclassified	Unclassified	Unclassified	

NSN 7540-01-280-5500

Standard Form 298 (Rev. 2-89)
Prescribed by ANSI Std. Z39-18
298-102